Utrecht University

Master's thesis

Institute for Theoretical Physics

Effective fluid parameters in a spherical universe

June 30, 2015

Author
Stella Boeschoten

Supervisor
Dr. E. Pajer
Institute for Theoretical Physics
Utrecht University

Universiteit Utrecht

Contents

Introduction **1**

Acknowledgements **3**

I Theoretical Background 5

1 Standard Perturbation Theory **7**
1.1 Equations of motion in real space . . . 8
1.2 Equations of motion in Fourier space . . . 9
1.3 Correlation functions . . . 12
1.3.1 Initial conditions . . . 13
1.3.2 The matter power spectrum . . . 13

2 Effective Field Theory of Large Scale Structures **17**
2.1 Smoothing . . . 18
2.2 Symmetries . . . 19
2.2.1 Self-similarity . . . 20

3 Spherical Collapse **23**
3.1 Parametric solutions . . . 23
3.2 Virialization . . . 24
3.3 Self-similarity in spherical collapse . . . 26

4 Past and Future Experiments **27**
4.1 The galaxy distribution . . . 27
4.1.1 From galaxy distribution to matter distribution . . . 27
4.1.2 Baryon acoustic oscillations . . . 28
4.1.3 Redshift-space distortions . . . 28
4.2 Past experiments . . . 29
4.3 Ongoing experiments . . . 30
4.4 Future experiments . . . 30
4.4.1 Outlook . . . 31

II Calculations 33

5 Calculation of c_s^2 using PT **35**
5.1 Third order perturbation theory . . . 35

6 Calculation of c_s^2 using SC **41**

Conclusion and Outlook **45**

A Alternative derivation of c_s^2 **47**
A.1 Cancellation of the P_{13} UV-divergence 51

Bibliography **52**

Introduction

One of the most interesting questions to ask when looking at our universe is the question of why the matter is distributed the way it is. How did galaxies develop, and then group together in clusters and superclusters? When and how did the matter distribution start to deviate from a homogeneous distribution? What is the history of our universe? What are its constituents? What is the nature of dark matter and dark energy?

In order to answer these questions, it is necessary to do observations and develop theories. Until recently, the cosmic microwave background (CMB) has been the leading cosmological observable. The CMB has given us reason to adapt the inflationary Big Bang model as the standard cosmological model. In this model, the distribution of matter started out almost completely uniform, with primordial perturbations of the order 10^{-5}. These primordial perturbations were then stretched out by a period of accelerated expansion in the primordial universe, called inflation. With the help of gravity, these small differences in density then caused the formation of large-scale structures. However, many details are still unclear and there are several different models for inflation that could all be true. Finding out whether the initial conditions from the primordial universe obey a Gaussian distribution or whether there exist small non-Gaussianities could help to distinguish between different inflationary models. By looking at the universe around us today, information about its very early form and its initial conditions can be extracted, thus making more observations is the key to learning more about our universe. However, the CMB has been extensively measured and analyzed and as of today, almost all useful information has been extracted from it. Fortunately, there is another way of making observations, namely using large-scale structure surveys. From the data that is collected with these surveys, we can extract a lot of still unexploited information, and thus the large-scale structures have the potential of becoming the next leading cosmological observable. One of the big advantages of these surveys over CMB surveys is the fact that they can be used to construct a three-dimensional map of the matter distribution, which contains a lot more information compared to the two-dimensional CMB maps. Also, the surveys have significantly improved over the last years because of new instrumentation that enables multiple galaxy spectra to be measured at once, and it is expected that they will become even better in the near future. More and more galaxy surveys are being performed, measuring millions of galaxies on large parts of the sky. In order to handle all this data, it is necessary to develop theories that are more accurate as well in order to be able to make predictions and confirm observations. The concepts of baryon acoustic oscillations and redshift-space distortions can help with the interpretation.

Several theories explaining large-scale structures have been proposed over the course of the years. The most famous one is the Standard Perturbation Theory (SPT). In this theory, the equations of motion are expanded in terms of density fluctuations, since these are expected to be small on large scales when assuming a homogeneous universe. SPT gives a good description of large-scale structure formation in the linear regime, but it breaks down on non-linear scales because density fluctuations become large such that perturbation theory is not possible anymore. Furthermore, loop integrals appear in the theory containing UV-divergences that cannot be renormalized. Hence, the theory becomes cut-off dependent. For a long time, SPT has been accurate enough to make suitable predictions. However, as mentioned above, in the past years, experimental power has significantly increased, thus more accurate theories are necessary. A few years ago, such a theory has been proposed. It is called the Effective Field

Theory of Large Scale Structures (EFToLSS). In this theory, the universe is modelled as an imperfect fluid with some effective parameters, namely viscosity, speed of sound, stochastic noise and infinitely many others that belong to higher order terms and are usually neglected. In this theory, a distinction is made between short scales and long scales. Long wavelength perturbations are expected to be small, thus these are treated linearly. However, short modes can become large, for example at the level of galaxies, and are thus difficult to work with. Thus, these short modes are "integrated out" of the theory. This means that we will first apply a smoothing to the equations of motion, hereby constructing a separation between long and short modes. Afterwards, the short modes are still random variables which are hard to treat, thus they are approximated by their average value plus some fluctuations. This results in the aforementioned effective terms, namely the average value gives rise to the speed of sound and viscosity and the fluctuations give rise to the stochastic noise. Through this procedure, the effect of the short modes on the long modes is systematically incorporated and the short modes do not appear in the theory explicitly anymore. One of the consequences is that the overdensity field becomes small everywhere and thus becomes a suitable expansion parameter. Furthermore, by using this approach, the effect of mode-coupling, which was neglected in SPT, is taken into account. Namely, at non-linear scales two short modes can couple to form a long mode, thus non-linear fluctuations could give small backreaction effects on the evolution of large-scale structures. Finally, the effective terms turn out to exactly cancel the aforementioned divergent terms of SPT. Thus, the EFToLSS tackles several of the problems of SPT. Because of these improvements, EFToLSS is able to make more precise predictions and help us to obtain a better understanding of large-scale structure formation.

Unfortunately, the effective parameters arising in the EFToLSS cannot be obtained from within the theory, since the equations of motion cannot be solved exactly. Thus, these parameters can only be determined through experiments or simulations. In this thesis, we concentrate on two of these parameters, namely the speed of sound c_s^2 and the viscosity c_v^2. These parameters only appear in the combination $c^2_{\text{comb}} = c_s^2 + c_v^2$ and thus cannot be measured separately. We would like to obtain an understanding of where these parameters come from and how they depend on time. In order to achieve this, first we will follow the perturbative approach that is used in EFToLSS. This allows us to check whether the speed of sound and viscosity terms indeed cancel one of the divergent terms arising in SPT. Then, we try to explicitly calculate c^2_{comb} from the equations of motion, using a simplifying assumption that will allow us to solve the equations of motion exactly. Namely, we will assume that all matter is distributed in a spherically symmetric way. Using the exact solutions obtained in this way, it is possible to construct the effective stress-energy tensor of which c^2_{comb} forms a part.

This thesis is divided into two parts. Part I consists of four chapters and contains all the relevant theoretical background that is needed to do the calculations in the next part. First, in Chapter 1, we summarize the important concepts of SPT, including the equations of motion and the power spectra. In Chapter 2 we proceed to the Effective Field Theory of Large Scale Structures (EFToLSS) and describe how it arises from SPT. Then, in Chapter 3, we treat the spherical collapse model, in which spherical symmetry is assumed during the process of gravitational collapse. We conclude the first part with Chapter 4, which consists of a description on how to actually perform large-scale structure experiments. Moreover, it contains an overview of important experiments from the past and experiments that are planned for the future.

Part II consists of two chapters. In Ch. 5, we use the concepts of perturbation theory to obtain an expression for the speed of sound. Finally, in Ch. 6, we attempt to give an explicit expression for the speed of sound, using the simplifying spherical collapse dynamics.

Acknowledgements

First of all, I would like to thank my supervisor Enrico Pajer. Our weekly meetings were always interesting and he has challenged me to really try to understand the physical implications of all the mathematics that we have been doing. He taught me to never just accept an equation, or a plot, or a theory, but to always ask myself where it is coming from and whether it makes sense intuitively. Because of this, I developed a much better physical intuition. Furthermore, I am grateful to the members of the cosmology journal club, for giving me the feeling that I belonged to a research group. Through our weekly journal clubs and monthly meetings in different cities, I experienced what it is like to do research and be part of an international community. Last but not least, I would like to thank my fellow master student Nikki Bisschop, with whom I have been working together during the whole year. Often, we were stuck together deriving some complicated equation, but many times we were able to help each other seeing something that the other person overlooked.

Part I

Theoretical Background

Chapter 1

Standard Perturbation Theory

The formation of large-scale structures in our universe is most likely caused by gravitational instability. Initial overdensities originating from the primordial universe are very small, of the order 10^{-5}, and still they will accumulate enough matter and structures will form. Schematically, the equation governing the growth of an overdensity δ is

$$\ddot{\delta} + [\text{Pressure} - \text{Gravity}]\delta = 0, \tag{1.1}$$

thus pressure and gravity act in opposite directions. Random thermal motion (pressure) drives matter out of the overdense region, while gravity attracts matter into it. If pressure is larger than gravity, the overdensity will oscillate and inhomogeneities do not grow. If gravity dominates, δ grows exponentially and structures will form. This is illustrated in Fig. 1.1 [1].

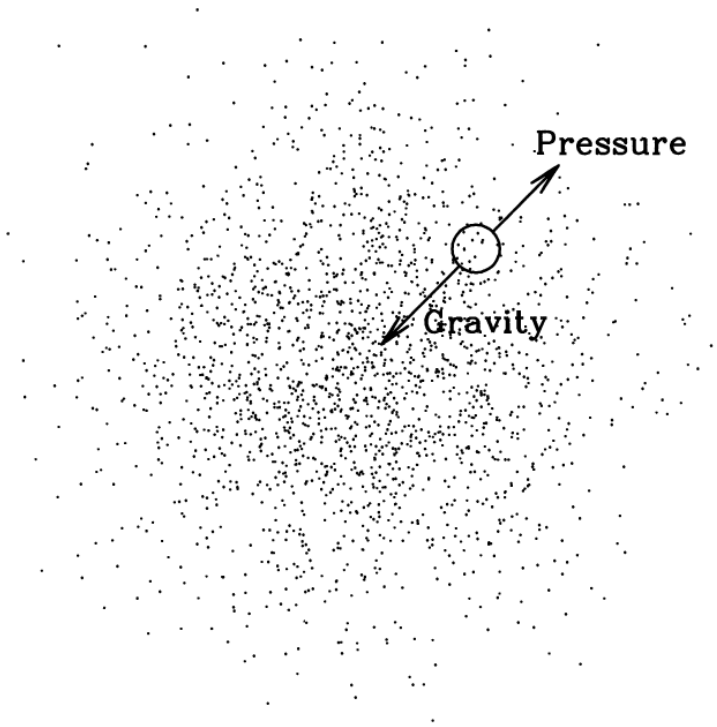

Figure 1.1: Gravitational instability: pressure and gravity act in opposite directions [1]

In our universe, the Hubble flow also needs to be taken into account. Whether fluctuations in the dark matter density will eventually collapse or will expand with the Hubble flow is determined by the so-called Jeans scale. The Jeans radius of an overdense region is the radius for which pressure and gravity exactly cancel each other. Thus, if an overdensity is smaller than the Jeans scale, it will not collapse and the collisionless dark matter particles are supported by their internal random velocities. On the other hand, if an overdensity is larger than the Jeans scale, it will grow under the influence of gravity. The rate at which the overdensity grows is independent of its scale. At matter-radiation equality, the Jeans scale is of the order of the horizon while deep in the matter domination era it approaches zero, because the pressure induced by radiation becomes smaller as matter becomes more dominant. During radiation domination, the Jeans scale was very large, thus structures did not form. The Jeans scale has had a lot of influence on the large-scale distribution of matter perturbations, which can be measured with galaxy surveys. In these surveys, what we measure is how the linear field produced during inflation looks today [2]. We will elaborate more on galaxy surveys in Ch. 4.

The equations describing the process of gravitational collapse are non-linear and thus very hard to solve. In order to try to understand the dynamics of gravitational instability in a quantitative way, cosmological perturbation theory can be used. Perturbation theory is possible because density fluctuations become sufficiently small on large scales, such that the overdensity can be used as an expansion parameter. In the framework in which cosmological perturbation theory has been developed, it is assumed that the universe is homogeneous and isotropic. Structure formation is explained by gravitational amplification of small primordial fluctuations of collisionless cold dark matter particles in an expanding universe. Furthermore, gravity is assumed to be the only process that causes structure formation.

1.1 Equations of motion in real space

The distribution function of cold dark matter in phase space, $f(\mathbf{x}, \mathbf{p}, \tau)$, obeys the Vlasov equation, which is the main equation of this chapter. Before we proceed to this equation, some definitions are in order. Because the universe is expanding and we only care about departures from this homogeneous Hubble expansion, we work in so-called comoving coordinates $\mathbf{x}$ that are related to the physical coordinates $\mathbf{r}$ through $\mathbf{r} = a(\tau)\mathbf{x}$, where $a(\tau)$ is the scale factor, written in terms of conformal time τ. Conformal time is related to cosmic time through $dt = a(\tau)d\tau$. Then we define the density contrast $\delta(\mathbf{x})$, the peculiar velocity $\mathbf{v}$ and the cosmological gravitational potential ϕ as follows (following [3]):

$$\begin{aligned} \rho(\mathbf{x}, \tau) &\equiv \bar{\rho}(\tau)[1 + \delta(\mathbf{x}, \tau)] \\ \mathbf{u}(\mathbf{x}, \tau) &\equiv \mathcal{H}\mathbf{x} + \mathbf{v}(\mathbf{x}, \tau) \\ \Phi(\mathbf{x}, \tau) &\equiv -\frac{1}{2}\frac{\partial \mathcal{H}}{\partial \tau}x^2 + \phi(\mathbf{x}, \tau), \end{aligned} \tag{1.2}$$

where $\bar{\rho}(\tau)$ is the homogeneous background density, $\rho(\mathbf{x}, \tau)$ the matter density, $\mathbf{u}$ the velocity of a particle, Φ the Newtonian potential, $\mathcal{H} \equiv d\ln a/d\tau = Ha$ the conformal expansion rate and H the Hubble rate. The velocity $\mathbf{u}$ and the peculiar velocity $\mathbf{v}$ differ in the respect that the latter does not include the movement of a particle as a result of the Hubble flow. Furthermore, ϕ is defined in such a way that it only depends on density fluctuations, namely the Poisson equation reads

$$\nabla^2\phi(\mathbf{x}, \tau) = \frac{3}{2}\Omega_m(\tau)\mathcal{H}^2(\tau)\delta(\mathbf{x}, \tau), \tag{1.3}$$

where $\Omega_m(\tau) = 8\pi G\bar{\rho}(\tau)/3H^2$ is the mass density parameter. The Vlasov equation in comoving coordinates is then given by

$$\frac{df}{d\tau} = \frac{\partial f}{\partial \tau} + \frac{\mathbf{p}}{ma} \cdot \nabla f - am\nabla\phi \cdot \frac{\partial f}{\partial \mathbf{p}} = 0, \tag{1.4}$$

where $\mathbf{p} = am\mathbf{v}$ is comoving momentum and m is the mass of a particle.

The Vlasov equation is very difficult to solve, since it is a non-linear partial differential equation involving seven variables. However, it is possible to derive two useful equations from the Vlasov equation, namely the continuity equation and the Euler equation. This can be done by *taking moments*. The zeroth, first and second moment of the phase space distribution function are defined as

$$\begin{aligned} \rho(\mathbf{x},\tau) &\equiv \int d^3\mathbf{p}\ f(\mathbf{x},\mathbf{p},\tau) \\ \rho(\mathbf{x},\tau)\mathbf{v}(\mathbf{x},\tau) &\equiv \int d^3\mathbf{p}\ \frac{\mathbf{p}}{am} f(\mathbf{x},\mathbf{p},\tau) \\ \rho(\mathbf{x},\tau)\mathbf{v}_i(\mathbf{x},\tau)\mathbf{v}_j(\mathbf{x},\tau) + \sigma_{ij}(\mathbf{x},\tau) &\equiv \int d^3\mathbf{p}\ \frac{p_i p_j}{a^2 m^2} f(\mathbf{x},\mathbf{p},\tau), \end{aligned} \tag{1.5}$$

where $\sigma_{ij}(\mathbf{x},\tau)$ is the velocity dispersion, which characterizes the deviation of particle motions from a single coherent flow $\mathbf{v}$. Now, we can also take moments of the whole Vlasov equation. The zeroth moment, obtained by integrating the Vlasov equation over momentum, gives the continuity equation,

$$\frac{\partial \delta(\mathbf{x},\tau)}{\partial \tau} + \nabla \cdot \{[1+\delta(\mathbf{x},\tau)]\mathbf{v}(\mathbf{x},\tau)\} = 0, \tag{1.6}$$

and the zeroth and first moments combined give the Euler equation,

$$\frac{\partial \mathbf{v}(\mathbf{x},\tau)}{\partial \tau} + \mathcal{H}(\tau)\mathbf{v}(\mathbf{x},\tau) + \mathbf{v}(\mathbf{x},\tau)\cdot\nabla\mathbf{v}(\mathbf{x},\tau) = -\nabla\phi(\mathbf{x},\tau) - \frac{1}{\rho}\nabla_j(\rho\sigma_{ij}). \tag{1.7}$$

The continuity and Euler equation respectively describe conservation of mass and conservation of momentum. All moment equations together are also called the Boltzmann hierarchy. All these moment equations are coupled: in the zeroth moment, $\mathbf{v}(\mathbf{x},\tau)$ appears, which has to be solved from the first moment equation, but in the first moment equation σ_{ij} appears which has to be solved from the second moment equation, and so on. Thus, to solve the theory exactly, one would need all moment equations. To solve this problem, we can for example make an ansatz for σ_{ij} in terms of $\mathbf{v}$. In standard perturbation theory, we will even neglect σ_{ij}, since deviations of particle motions from a single coherent flow $\mathbf{v}$ are expected to be small in the first stages of gravitational collapse. In EFToLSS, as we will see in Ch. 2, it is straightforward to take this term into account thus it is not necessary to neglect it anymore.

Furthermore, we will also neglect vorticity, $\nabla\times\mathbf{v}$, since we assume that initially there is no vorticity and then the equations of motion guarantee that it will remain zero until shell-crossing (which does not occur until the final stages of gravitational collapse). Even if there would be nonzero vorticity, it would quickly decay since $\nabla\times\mathbf{v}\propto a^{-1}$. This can be easily seen by taking the curl of Eq. 1.7 to obtain an equation in terms of the vorticity.

Using these assumptions, we can rewrite the equations of motion in terms of $\delta(\mathbf{x},\tau)$ and the velocity divergence $\theta(\mathbf{x},\tau) = \nabla\cdot\mathbf{v}(\mathbf{x},\tau)$. Because of the perturbative approach, we assume that it is possible to expand these fields about the linear solutions, which means that the variance of the linear fluctuations is treated as a small parameter,

$$\delta(\mathbf{x},\tau) = \sum_{n=1}^{\infty}\delta^{(n)}(\mathbf{x},\tau), \qquad \theta(\mathbf{x},\tau) = \sum_{n=1}^{\infty}\theta^{(n)}(\mathbf{x},\tau), \tag{1.8}$$

thus $\delta^{(1)}$ and $\theta^{(1)}$ are linear in the initial density field, $\delta^{(2)}$ and $\theta^{(2)}$ are quadratic, and so on.

1.2 Equations of motion in Fourier space

To proceed, it is useful to convert our equations to Fourier space. In the linear regime, different Fourier modes evolve independently conserving the primordial statistics. In the non-linear regime on

the other hand, the equations of motion clearly show the coupling between different Fourier modes. The equations of motion in Fourier space become (again following [3])[1]

$$\frac{\partial\tilde{\delta}(\mathbf{k},\tau)}{\partial\tau}+\tilde{\theta}(\mathbf{k},\tau)=-\int_{\mathbf{k}_1,\mathbf{k}_2}\delta_D(\mathbf{k}-\mathbf{k}_{12})\alpha(\mathbf{k}_1,\mathbf{k}_2)\tilde{\theta}(\mathbf{k}_1,\tau)\tilde{\delta}(\mathbf{k}_2,\tau), \tag{1.11}$$

$$\begin{aligned}\frac{\partial\tilde{\theta}(\mathbf{k},\tau)}{\partial\tau}+\mathcal{H}(\tau)\tilde{\theta}(\mathbf{k},\tau)+\frac{3}{2}\Omega_m\mathcal{H}^2(\tau)\tilde{\delta}(\mathbf{k},\tau)=\\ -\int_{\mathbf{k}_1,\mathbf{k}_2}\delta_D(\mathbf{k}-\mathbf{k}_{12})\beta(\mathbf{k}_1,\mathbf{k}_2)\tilde{\theta}(\mathbf{k}_1,\tau)\tilde{\theta}(\mathbf{k}_2,\tau),\end{aligned} \tag{1.12}$$

where

$$\alpha(\mathbf{k}_1,\mathbf{k}_2)\equiv\frac{\mathbf{k}_{12}\cdot\mathbf{k}_1}{k_1^2},\qquad\beta(\mathbf{k}_1,\mathbf{k}_2)\equiv\frac{k_{12}^2(\mathbf{k}_1\cdot\mathbf{k}_2)}{2k_1^2k_2^2} \tag{1.13}$$

and $\mathbf{k}_{12}=\mathbf{k}_1+\mathbf{k}_2$. The terms on the right hand side come from the non-linear terms in the continuity and Euler equation. These terms describe the mode-coupling. We see that there is only mode-coupling between modes with wave-vectors whose sum is $\mathbf{k}$, which should indeed be the case in a spatially homogeneous universe because of translational invariance.

We will now specify our universe to be Einstein-de Sitter (EdS), thus $\Omega_m=1$, $\Omega_\Lambda=0$, $a(\tau)\propto\tau^2$ and $\mathcal{H}(\tau)=2/\tau$. This describes a flat universe which only contains dark and baryonic matter. In the following chapters, we will often approximate our universe to be Einstein-de Sitter. It is clear that our universe is actually more complicated than that, but it is a good approximation as long as the universe is matter-dominated. In Fig. 1.2, it can be seen when this is the case. In EdS, the equations of motion are solved by

$$\tilde{\delta}(\mathbf{k},\tau)=\sum_{n=1}^{\infty}a^n(\tau)\delta_n(\mathbf{k}),\qquad\tilde{\theta}(\mathbf{k},\tau)=-\mathcal{H}(\tau)\sum_{n=1}^{\infty}a^n(\tau)\theta_n(\mathbf{k}). \tag{1.14}$$

In these solutions, only the growing mode is taken into account, since the other mode is decaying and can thus be neglected. From the continuity equation it follows that $\delta_1(\mathbf{k})=\theta_1(\mathbf{k})$, thus at linear order $\tilde{\delta}(\mathbf{k},\tau)=a\delta_1(\mathbf{k})$ and $\tilde{\theta}(\mathbf{k},\tau)=-\mathcal{H}(\tau)a(\tau)\delta_1(\mathbf{k})$. Plugging these perturbative solutions into Eqs. (1.11) and (1.12), we obtain expressions for $\delta_n(\mathbf{k})$ and $\theta_n(\mathbf{k})$ in terms of the linear fluctuations $\delta_1(\mathbf{k})$:

$$\delta_n(\mathbf{k})=\int_{\mathbf{q}_1,\ldots,\mathbf{q}_n}\delta_D(\mathbf{k}-\mathbf{q}_{1\ldots n})F_n(\mathbf{q}_1,\ldots,\mathbf{q}_n)\delta_1(\mathbf{q}_1)\ldots\delta_1(\mathbf{q}_n), \tag{1.15}$$

$$\theta_n(\mathbf{k})=\int_{\mathbf{q}_1,\ldots,\mathbf{q}_n}\delta_D(\mathbf{k}-\mathbf{q}_{1\ldots n})G_n(\mathbf{q}_1,\ldots,\mathbf{q}_n)\delta_1(\mathbf{q}_1)\ldots\delta_1(\mathbf{q}_n), \tag{1.16}$$

where the kernels are given by the recursion relations

$$\begin{aligned}F_n(\mathbf{q}_1,\ldots,\mathbf{q}_n)=\sum_{m=1}^{n-1}\frac{G_m(\mathbf{q}_1,\ldots,\mathbf{q}_m)}{(2n+3)(n-1)}[(2n+1)\alpha(\mathbf{k}_1,\mathbf{k}_2)F_{n-m}(\mathbf{q}_{m+1},\ldots,\mathbf{q}_n)\\ +2\beta(\mathbf{k}_1,\mathbf{k}_2)G_{n-m}(\mathbf{q}_{m+1},\ldots,\mathbf{q}_n)],\end{aligned} \tag{1.17}$$

[1] We use the following notation for the real- and momentum-space integrals:

$$\int_{\mathbf{x}}\equiv\int d^3\mathbf{x},\qquad\int_{\mathbf{p}}\equiv\int\frac{d^3\mathbf{p}}{(2\pi)^3}, \tag{1.9}$$

and the following convention for the Fourier transform:

$$\tilde{A}(\mathbf{k},\tau)=\int_{\mathbf{x}}e^{-i\mathbf{k}\cdot\mathbf{x}}A(\mathbf{x},\tau),\qquad A(\mathbf{x},\tau)=\int_{\mathbf{k}}e^{i\mathbf{k}\cdot\mathbf{x}}\tilde{A}(\mathbf{k},\tau). \tag{1.10}$$

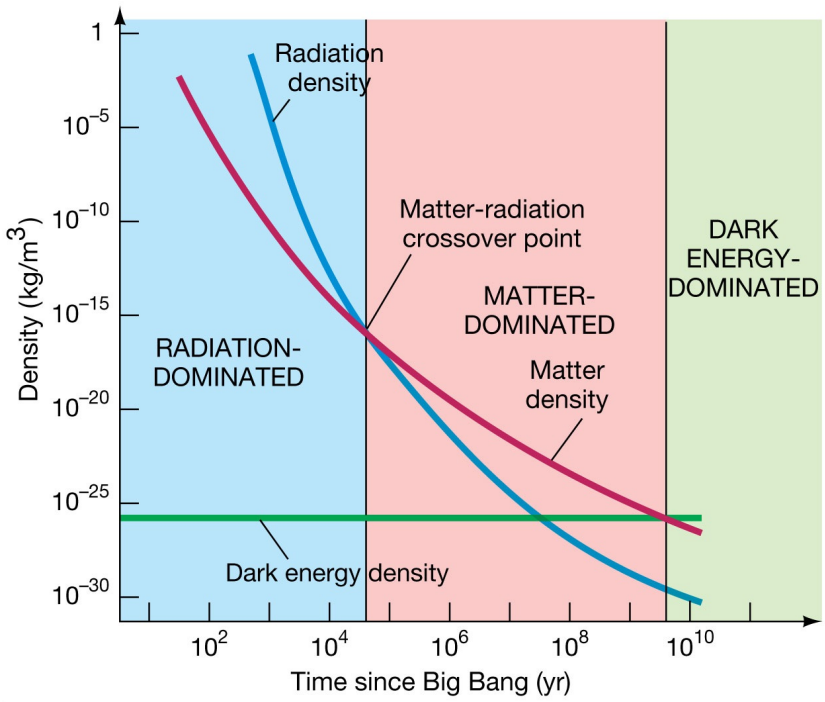

Figure 1.2: Evolution of the matter-, radiation- and dark energy density. The colors indicate the period of time in which one of the three components dominates [4].

$$G_n(\mathbf{q}_1,\ldots,\mathbf{q}_n) = \sum_{m=1}^{n-1} \frac{G_m(\mathbf{q}_1,\ldots,\mathbf{q}_m)}{(2n+3)(n-1)}[3\alpha(\mathbf{k}_1,\mathbf{k}_2)F_{n-m}(\mathbf{q}_{m+1},\ldots,\mathbf{q}_n) + 2n\beta(\mathbf{k}_1,\mathbf{k}_2)G_{n-m}(\mathbf{q}_{m+1},\ldots,\mathbf{q}_n)], \tag{1.18}$$

where $\mathbf{k}_1 \equiv \mathbf{q}_1 + \cdots + \mathbf{q}_m$, $\mathbf{k}_2 \equiv \mathbf{q}_{m+1} + \cdots + \mathbf{q}_n$ and $F_1 = G_1 \equiv 1$. Often, we will use the symmetrized kernels $F_n^{(s)}$ and $G_n^{(s)}$, obtained by a normalized summation of F_n and G_n over all possible permutations of the variables. If we take the spherical average over the above kernels, we obtain the coefficients ν_n and μ_n, defined as

$$\begin{aligned} \nu_n &\equiv n! \int \frac{d\Omega_1}{4\pi} \ldots \frac{d\Omega_n}{4\pi} F_n(\mathbf{k}_1,\ldots,\mathbf{k}_n), \\ \mu_n &\equiv n! \int \frac{d\Omega_1}{4\pi} \ldots \frac{d\Omega_n}{4\pi} G_n(\mathbf{k}_1,\ldots,\mathbf{k}_n), \end{aligned} \tag{1.19}$$

and it turns out that these coefficients can be used to write a solution for δ in which spherical collapse dynamics is assumed, namely by using Eq. 1.15 and transforming back to real space, we write

$$\delta_{sc}(x,a) = \sum_n a^n \int_{\mathbf{x},\mathbf{q}_1,\ldots,\mathbf{q}_n} \delta_D(\mathbf{k}-\mathbf{q}_{1\ldots n}) F_n(\mathbf{q}_1,\ldots,\mathbf{q}_n)\delta_1(|\mathbf{q}_1|)\ldots\delta_1(|\mathbf{q}_n|)e^{i\mathbf{k}\cdot\mathbf{x}}, \tag{1.20}$$

where δ_1 now only depends on the magnitude of its argument because of spherical symmetry. Then performing the angular integral and the $\mathbf{x}$-integral, the integrals over $\mathbf{q}_1,\ldots,\mathbf{q}_n$ decouple and can be written as a product. We obtain

$$\begin{aligned} \delta_{sc}(x,a) &= \sum_n \frac{\nu_n}{n!} a^n \left(\int_{\mathbf{q}} \delta_1(q) e^{i\mathbf{q}\cdot\mathbf{x}} \right)^n \\ &= \sum_n \frac{\nu_n}{n!} a^n [\delta_1(x)]^n, \end{aligned} \tag{1.21}$$

where

$$\nu_1 = \mu_1 = 1; \quad \nu_2 = \frac{34}{21}; \quad \nu_3 = \frac{682}{189}; \quad \mu_2 = -\frac{26}{21}; \quad \mu_3 = \frac{142}{63}. \tag{1.22}$$

A similar expansion holds for the velocity divergence in terms of the coefficients μ_n. Thus, the angular averages of the kernels from perturbation theory are related to spherical collapse dynamics [3]. We will use this fact in Ch. 6.

1.3 Correlation functions

In order to understand the evolution of large-scale structures, correlation functions can be used. Correlation functions are given by expectation values over combinations of overdensity fields, and thus they relate overdensities at certain points to overdensities at other points. The two-point correlation function is defined as

$$\xi(r) = \langle \delta(\mathbf{x})\delta(\mathbf{x}+\mathbf{r})\rangle, \tag{1.23}$$

where $\langle \dots \rangle$ represents the joint ensemble average. $\xi(r)$ only depends on the difference $(\mathbf{x}+\mathbf{r})-\mathbf{x} = \mathbf{r}$ and only on the norm because of *statistical homogeneity and isotropy*. Statistical homogeneity means that all probability distribution functions only depend on relative positions and statistical isotropy means that these functions are also invariant under spatial rotations. Most cosmological theories predict that cosmic fields possess these properties.

In order to obtain an intuitive understanding of what a correlation function actually is, let us consider two small regions of respective volumes δV_1 and δV_2, separated by a distance r. Then the expected number of *pairs* of galaxies of which one galaxy is lying in region 1 and the other one in region 2 is given by [2]

$$\langle n_{\text{pair}}\rangle = \bar{n}^2[1+\xi(r)]\delta V_1 \delta V_2, \tag{1.24}$$

where $\bar{n}$ is the mean number of galaxies per unit volume. From the equation for $\langle n_{\text{pair}}\rangle$ it is easy to see that $\xi(r)$ gives an expression for the excess clustering of galaxies at a separation r. If $\xi(r) > 0$, this corresponds to strong clustering, and vice versa for $\xi(r) < 0$. If $\xi(r) = 0$, the galaxies are unclustered. In Fourier space, note that $\delta(\mathbf{k}) = \delta^*(-\mathbf{k})$ because $\delta(\mathbf{x})$ is real, and the correlation function becomes

$$\begin{aligned}
\langle \delta(\mathbf{k})\delta(\mathbf{k}')\rangle &= \int_{\mathbf{x},\mathbf{r}} \langle \delta(\mathbf{x})\delta(\mathbf{x}+\mathbf{r})\rangle e^{-i(\mathbf{k}+\mathbf{k}')\cdot\mathbf{x} - i\mathbf{k}'\cdot\mathbf{r}} \\
&= \int_{\mathbf{x},\mathbf{r}} \xi(r) e^{-i(\mathbf{k}+\mathbf{k}')\cdot\mathbf{x} - i\mathbf{k}'\cdot\mathbf{r}} \\
&= (2\pi)^3 \delta_D(\mathbf{k}+\mathbf{k}') \int_{\mathbf{r}} \xi(r) e^{i\mathbf{k}\cdot\mathbf{r}} \\
&\equiv (2\pi)^3 \delta_D(\mathbf{k}+\mathbf{k}') P(k),
\end{aligned} \tag{1.25}$$

where $P(k)$ is the so-called *power spectrum*. The power spectrum $P(k)$ and the two-point correlation function $\xi(r)$ form a Fourier pair and thus contain the same information. Furthermore, we define the dimensionless power spectrum [3]

$$\Delta^2(k) \equiv \frac{k^3}{2\pi^2} P(k). \tag{1.26}$$

N-point functions P_N are defined analogously to the 2-point function:

$$(2\pi)^3 \delta_D(\mathbf{k}_1 + \dots + \mathbf{k}_N) P_N(\mathbf{k}_1, \dots, \mathbf{k}_N) = \langle \delta(\mathbf{k}_1) \dots \delta(\mathbf{k}_N)\rangle. \tag{1.27}$$

The 3-point function is called the bispectrum and it is generally denoted by $B(k_1, k_2, k_3)$. The precise form of the N-point functions highly depends on the initial conditions, which will be explained in the next section.

1.3.1 Initial conditions

As mentioned before, the large-scale structures that we observe today are the result of the evolved primordial perturbations. The precise form of the initial conditions is very important for the shape of the present structures. These are the same initial conditions that are also responsible for the anisotropies in the cosmic microwave background, but since the CMB contains information from much earlier in the universe, it is easier to relate this information to the primordial universe compared to the information from LSS. Matter has evolved non-linearly for a long time thus it is hard to trace the present structures back to the primordial universe.

In order to learn more about the early universe, we want to know whether the primordial matter field contains non-Gaussianities. The leading-order departure from a Gaussian distribution is contained in the bispectrum of the gravitational potential. However, it is difficult to specify which non-Gaussianities in the present density distribution actually come from the primordial field, since there are two other sources of non-Gaussianity. First, the matter fields evolve non-linearly under the influence of gravity and this can introduce non-Gaussian correlations even if the primordial power spectrum is Gaussian. Second, there are non-linearities in the bias relation between the galaxy and matter distribution. This means that the bispectrum will be non-vanishing in any case and non-Gaussian initial conditions will only change its shape.

In the special case that the initial conditions are actually Gaussian, all higher-order correlation functions can be described in terms of two-point functions by using Wick's theorem, thus the two-point function or power spectrum completely describes the system. However, when initial conditions are non-Gaussian, extra terms appear in higher-order correlation functions. The power spectrum can be expanded as follows,

$$\langle\delta\delta\rangle = \langle(\delta_1+\delta_2+\delta_3+\ldots)^2\rangle \simeq \langle\delta_1\delta_1\rangle + 2\langle\delta_1\delta_2\rangle + \langle\delta_2\delta_2\rangle + 2\langle\delta_1\delta_3\rangle + \ldots. \tag{1.28}$$

In the case of Gaussian initial conditions, any correlation function over an odd number of δ_1 vanishes, thus e.g. $\langle\delta_1\delta_2\rangle \sim \langle\delta_1^3\rangle$ would be zero, since the linear overdensity δ_1 remains Gaussian at all times. For general initial conditions, this term leads to a correction to the power spectrum (following [3]),

$$P(k) = P^I(k) + 2\int_{\mathbf{q}} F_2(\mathbf{k}+\mathbf{q},-\mathbf{q})B^I(\mathbf{k},\mathbf{q}), \tag{1.29}$$

where P^I is the initial power spectrum and B^I the initial bispectrum ($B^I \sim \langle\delta_1^3\rangle$). Similarly, the bispectrum has a correction dependent on the trispectrum P_4^I, and so on. These correction terms are complicated because they contain a convolution with the second order kernel F_2. By looking at the shape of the bispectrum, we can extract information about the initial conditions. Thus, initial conditions can help us to distinguish between different inflationary models. For general initial conditions, the correction terms are typically divergent thus making the theory cut-off dependent. In this thesis, we assume that the initial conditions are Gaussian. Then, the power spectrum is the most important tool to describe large-scale structure formation. We will go into this a little more deeply in the next section.

1.3.2 The matter power spectrum

Roughly, there are three stages in the evolution of cosmological perturbations. First, we have the very early stage, in which all Fourier modes are still outside the horizon, $k\tau \ll 1$ where τ is conformal time, and the gravitational potential is constant. Then, the intermediate stage: in this stage, as the universe expands, modes start entering the horizon. Furthermore, the universe evolves from radiation domination to matter domination. Whether a mode crosses the horizon before or after matter-radiation equality greatly affects the potential, as can be seen in Fig. 1.3. A fluctuation that enters the horizon during radiation domination is effectively frozen until matter-radiation equality, because the radiation density acts as a kind of pressure that prevents perturbations in the matter density from collapsing

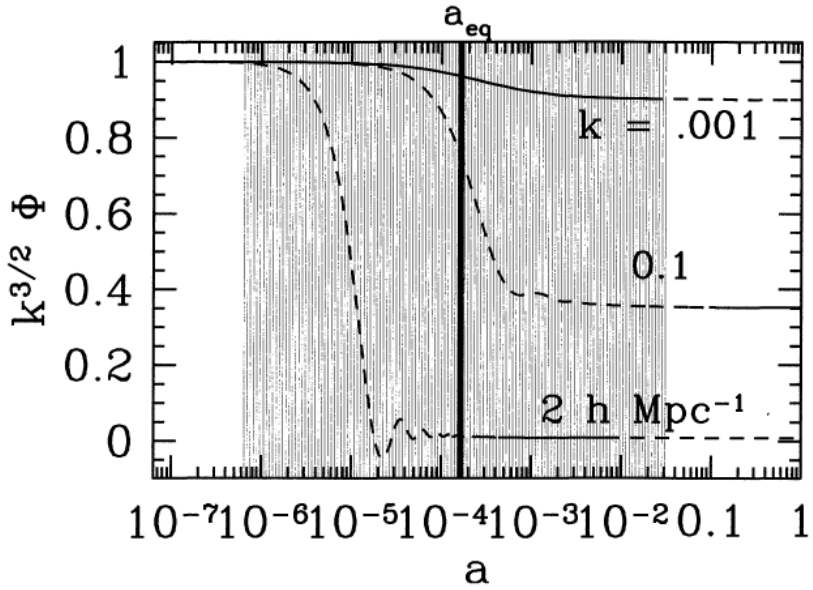

Figure 1.3: The linear evolution of the gravitational potential Φ, neglecting baryons and assuming $\Omega_m = 1$, $h = 0.5$. Three different modes have been plotted and the dashed lines denote when the mode enters the horizon [1].

[5]. The expansion of the universe is too fast for these matter overdensities to collapse. This is closely related to the Jeans scale, which was explained in the beginning of this chapter. It can for example be seen in Fig. 1.4 for the smallest scale $k = 2$ h Mpc^{-1}. At $a \sim 10^{-5}$, it enters the horizon and its growth is immediately retarded. This retardation ends again at $a \sim 10^{-4}$, when matter-radiation equality takes place. Finally, in the last stage, all modes evolve identically and for $\Omega_m = 1$, as plotted in Fig. 1.3, the potential even remains constant.

While doing experiments, what we observe is the latest stage. In order to relate this to the primordial potential that was generated during inflation, we can write

$$\Phi(\mathbf{k}, a) = \frac{9}{10}\Phi_p(\mathbf{k}) \times T(k) \times \frac{D_1(a)}{a}, \tag{1.30}$$

where $T(k)$ is the transfer function, $D_1(a)$ the linear growth function and Φ_p the primordial potential set during inflation [1]. Note that in EdS $D_1(a) = a$ and thus the potential indeed does not depend on a. The transfer function encapsulates the change in the power spectrum from the inflationary form to the power spectrum in the matter-dominated regime, while the growth function describes the wavelength-independent growth at late times. In Fig. 1.4, it can be seen that at late times, when the potential is constant and all modes are within the horizon, the growth of overdensities is solely described by the growth function. In EdS this boils down to $\delta \propto a$. Using Poisson's equation in the large-k limit and neglecting radiation, it can be shown that

$$\delta(\mathbf{k}, a) = \frac{3}{5}\frac{k^2}{\Omega_m H_0^2}\Phi_p(\mathbf{k})T(k)D_1(a). \tag{1.31}$$

This formula is valid for any Φ_p. Assuming Gaussian initial conditions for inflation, Φ_p is drawn from a Gaussian distribution. Using this, it is possible to obtain an explicit formula for the power spectrum, namely

$$P(k, a) = 2\pi^2\delta_H^2\frac{k^n}{H_0^{n+3}}T^2(k)\left(\frac{D_1(a)}{D_1(a=1)}\right)^2, \tag{1.32}$$

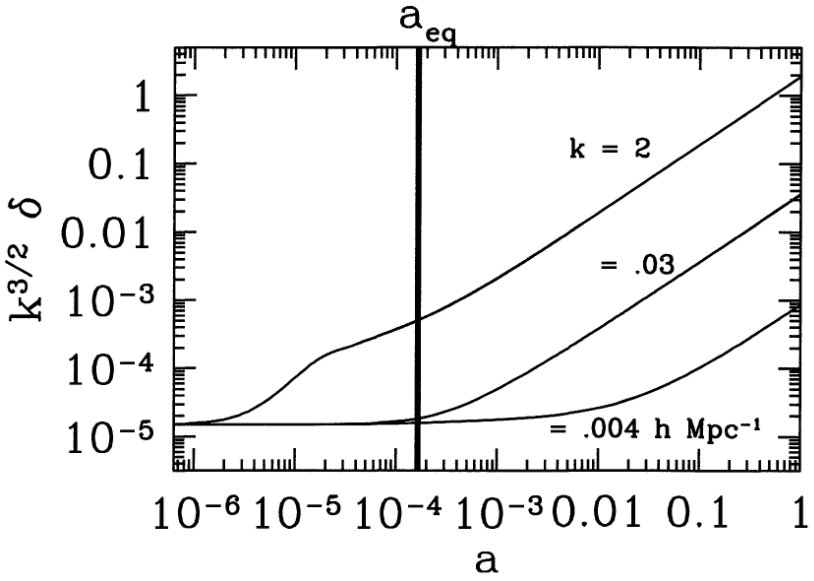

Figure 1.4: Evolution of dark matter perturbations, using the same model as in Fig. 1.3 [1].

where H_0 is the Hubble constant today, δ_H the scalar amplitude at horizon crossing and n the spectral index. $P(k,a)$ has dimension length^3. To make it dimensionless, we can switch to $\Delta^2(k)$, which was defined in Eq. 1.26. Then, small Δ corresponds to small perturbations and large Δ corresponds to non-linear overdensities. In the simplest inflationary model $n = 1$. This is plotted in Fig. 1.5. On large scales, the transfer function is unity and $P(k) \propto k$. On small scales, we see that the power spectrum turns over: it does not evolve linearly anymore. This turn-over happens at the horizon scale from matter-radiation equality, because from that point on the radiation pressure is not acting to prevent collapse anymore thus non-linear evolution becomes possible. This corresponds to the scale $k_{\rm NL}$, which is defined below. In Fig. 1.5, two different models are plotted, namely EdS, in which it is assumed that the universe contains only cold dark matter, and ΛCDM, in which there is also a cosmological constant Λ. For EdS, the turn-over takes place on smaller scales because in this model the universe contains more matter compared to ΛCDM and therefore it has a smaller $a_{\rm eq}$.

Non-linear scale

Perturbation theory breaks down when overdensities become non-linear. In order to have an idea of when this happens, we define $k_{\rm NL}$ as the scale above which non-linearities cannot be ignored. There are several ways to define $k_{\rm NL}$, for example through

$$\Delta^2(k_{\rm NL}) = 1, \tag{1.33}$$

from which it follows that at present time $k_{\rm NL} \simeq 0.2$ h Mpc^{-1} in most cosmological models. For a general universe the non-linear scale is always smaller than the scale of matter-radiation equality, which means that non-linear scales have entered the horizon during radiation-domination and were thus suppressed until matter-radiation equality. It is thus expected that these small-scale non-linearities do not have very large effects on the background evolution. Very small scales even turn out to give no effect at all if they correspond to virialized structures. For an EdS-universe, the main contribution from short scales comes from $q \sim k_{\rm NL}$, while for a universe containing matter and radiation, the main contribution comes from $q \sim k_{\rm eq}$ which corresponds to the scale of matter-radiation equality.

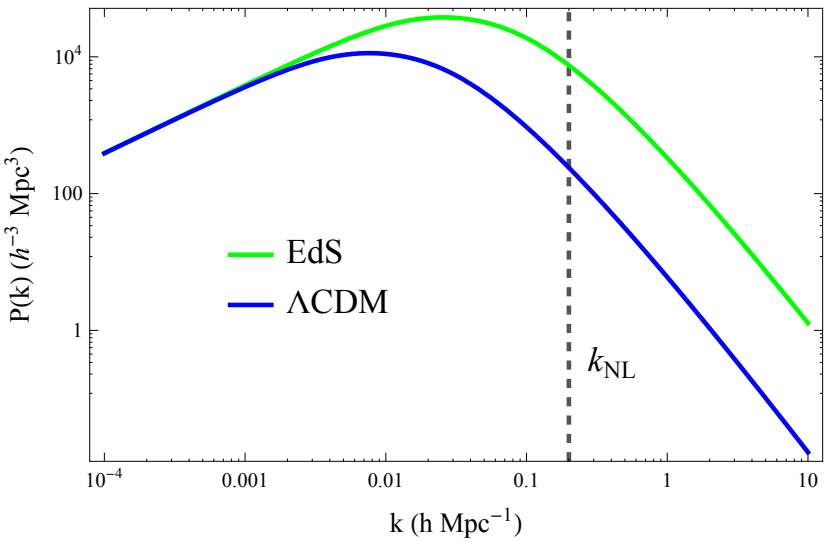

Figure 1.5: The power spectrum in two models, namely EdS ($\Omega_m = 1$, $\Omega_\Lambda = 0$) and ΛCDM ($\Omega_m = 0.3$, $\Omega_\Lambda = 0.7$). The vertical line is given by $k_{\rm NL}$, thus to the left of this line scales evolve linearly.

Chapter 2

Effective Field Theory of Large Scale Structures

The reason that standard perturbation theory as described in the previous chapter works very well is because of the large hierarchy between the two fundamental scales that characterize the formation of large-scale structures, namely $\epsilon = k_{NL}^{-1}/\mathcal{H}^{-1} \ll 1$. Here, k_{NL}^{-1} is the non-linear scale, as defined in Eq. 1.33, which characterizes the size of the structures whose density contrast exceeds unity, and $\mathcal{H}^{-1}$ is the Hubble scale, which characterizes the extent of the observable universe and thus limits the range over which interactions can influence the evolution of large-scale perturbations. This hierarchy shows that the size of significant structures is still much smaller than the Hubble scale, thus usually the universe is well approximated by perturbation theory with small density perturbations. Most observations can be explained in a satisfactory way within perturbation theory. However, as our observations become more advanced, a problem arises. Namely, small-scale non-linearities could actually induce a backreaction on the long-distance universe. This could happen through mode-coupling, since two short-wavelength Fourier modes can couple to form one long-wavelength perturbation. Corrections of this form can have an observable effect on structure formation. Because of the large hierarchy of scales, the problem can be tackled using an Effective Field Theory (EFT) approach. In general, effective theories are used to capture the important behaviour of a theory with many degrees of freedom via a description with far fewer degrees of freedom. In a field theory, variables are fields defined over space. An effective field theory is thus a theory in which the short scales are 'averaged out', such that those scales will only give an effect through various couplings in a perturbative expansion in ϵ [6] [7].

The effective field theory can be used to describe the long-distance universe on scales larger than the non-linear scale. In this theory, the universe is described as a fluid with small perturbations. At leading order, this fluid can be described as an ordinary imperfect fluid which is characterized by a speed of sound, a viscosity and a stochastic pressure. In order to determine these parameters from within the theory, one would have to solve the fully non-linear equations of motion. Since this is not possible, the parameters have to be determined through simulations or observations. These parameters give rise to some effective terms that were not present in SPT. This actually solves another problem, mentioned briefly in the introduction. Namely, in SPT, some of the final results like the density power spectrum are given in terms of a loop expansion. However, loop integrals are divergent for generic initial conditions and no terms appear that could cancel these divergences, see e.g. Eq. 1.29. It turns out that the effective terms arising in the EFToLSS have exactly the right scale- and time-dependence to cancel them, as we will show in Ch. 5 and App. A.

2.1 Smoothing

As in SPT, we again assume that dark matter is collisionless, classical and non-relativistic and that the only interaction causing structure formation is gravity. The equations of motion are derived from those of SPT by a procedure called smoothing. This procedure allows us to expand the velocity dispersion in terms of long-wavelength quantities, thus we are able to truncate the Boltzmann hierarchy. This results in an effective fluid. The Gaussian smoothing is defined as (see e.g. [7])

$$W_\Lambda(\mathbf{x}) = \left(\frac{\Lambda}{\sqrt{2\pi}}\right)^3 e^{-\frac{1}{2}\Lambda^2 x^2}, \qquad W_\Lambda(\mathbf{k}) = e^{-\frac{1}{2}\frac{k^2}{\Lambda^2}}, \tag{2.1}$$

where Λ is the cut-off scale. When applying this smoothing to a certain quantity, the result is that small scales $k > \Lambda$ are suppressed. Consequently, we define long-wavelength quantities as

$$\mathcal{O}_l(\mathbf{x},\tau) = [\mathcal{O}]_\Lambda(\mathbf{x},\tau) = \int_{\mathbf{x}'} W_\Lambda(\mathbf{x}-\mathbf{x}')\mathcal{O}(\mathbf{x}'). \tag{2.2}$$

Furthermore, a short-wavelength quantity or short mode is defined as $\mathcal{O}_s \equiv \mathcal{O} - \mathcal{O}_l$. The effect of smoothing is illustrated in Fig. 2.1.

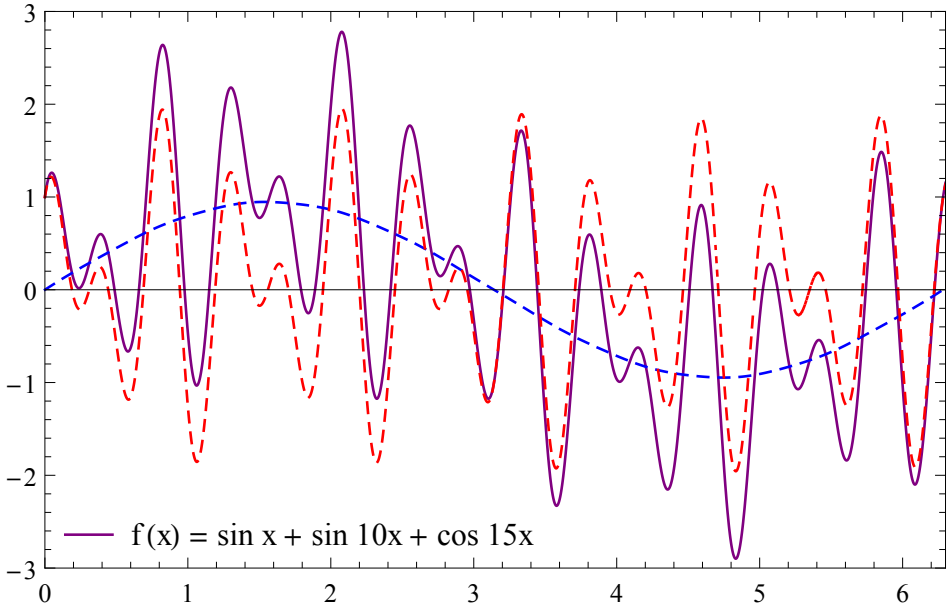

Figure 2.1: The effects of smoothing: the purple line describes the original function, the dashed blue line is the smoothed function or long mode and the dashed red line is the short mode, i.e., the original function minus the smoothed function.

We now apply the smoothing procedure to the Vlasov equation and take moments again, equivalent to the procedure in SPT. The equations of motion become

$$\partial_\tau \delta_l + \partial_i[(1+\delta_l)v_l^i] = 0, \tag{2.3}$$

$$\partial_\tau v_l^i + \mathcal{H} v_l^i + \partial_i \phi_l + v_l^k \partial_k v_l^i = -\frac{1}{\rho_l}\partial_j[\tau^{ij}]_\Lambda, \tag{2.4}$$

$$\partial^2 \phi_l = \frac{3}{2}\mathcal{H}^2 \Omega_m \delta_l, \tag{2.5}$$

where τ^{ij} is the effective stress-energy tensor which encapsulates the corrections induced by the short scales. This tensor explicitly depends on the short scales, which are still random variables that are strongly coupled and thus hard to treat within the effective theory. Because of this, we will take the expectation value of the stress-energy tensor over the short modes. This expectation value will still depend on the long modes, for example through tidal effects. However, because long wavelength fluctuations δ_l and v_l are small, we can perform a Taylor expansion in their size to obtain

$$\langle [\tau^{ij}]_\Lambda \rangle_{\delta_l} = \langle [\tau^{ij}]_\Lambda \rangle_0 + \left. \frac{\partial \langle [\tau^{ij}]_\Lambda \rangle_{\delta_l}}{\partial \delta_l} \right|_{\delta_l=0} \delta_l + \dots . \tag{2.6}$$

If we expand up to linear order in perturbations and to lowest order in derivatives and take into account the symmetries of the problem, we obtain

$$\langle [\tau^{ij}]_\Lambda \rangle_{\delta_l} = p_b \delta^{ij} + \rho_b \left[c_s^2 \delta_l \delta^{ij} - \frac{c_{bv}^2}{\mathcal{H}} \delta^{ij} \partial_k v_l^k - \frac{3}{4} \frac{c_{sv}^2}{\mathcal{H}} \left(\partial^j v_l^i + \partial^i v_l^j - \frac{2}{3} \delta^{ij} \partial_k v_l^k \right) \right] + \Delta\tau^{ij} + \dots , \tag{2.7}$$

where p_b is the background pressure induced by short distance inhomogeneities even in the absence of long wavelength fluctuations, c_s^2, c_{bv}^2 and c_{sv}^2 correspond to the speed of sound, bulk and shear viscosity and $\Delta\tau^{ij}$ represents the stochastic noise. In the remainder of this thesis, when we talk about c_s^2, we actually mean $c_s^2 + c_{bv}^2 + c_{sv}^2$ since it is the combination of these terms that is relevant at one-loop order. As mentioned in the introduction of this chapter, the effective terms arising from this effective stress-energy tensor will cancel the divergences in the power spectrum that are present in SPT. The one-loop power spectrum is given by [8]

$$P(k,a) = P_{\rm lin}(k,a) + P_{22}(k,a) + P_{13}(k,a) + P_{c_s^2}(k,a) + P_J(k,a) \tag{2.8}$$

where we defined $(2\pi)^3 \delta_D(\mathbf{k}+\mathbf{k}') P_{\rm lin}(k,a) = \langle \delta^{(1)}(\mathbf{k},a) \delta^{(1)}(\mathbf{k}',a) \rangle$, where $\delta^{(1)}(\mathbf{k},a) = a\delta_1(\mathbf{k})$ as in Ch. 1, and furthermore $(2\pi)^3 \delta_D(\mathbf{k}+\mathbf{k}') P_{13}(k,a) = \langle \delta^{(1)} \delta^{(3)} \rangle + \langle \delta^{(3)} \delta^{(1)} \rangle$ and similar definitions for the other power spectra. $P_{c_s^2}$ represents the contribution to the power spectrum that arises from c_s^2, c_{bv}^2 and c_{sv}^2 and P_J represents the contribution from $\Delta\tau^{ij}$. The linear power spectrum is related to the initial power spectrum through

$$P_{\rm lin}(k,a) = a^2 P_{\rm in}(k) \tag{2.9}$$

where $(2\pi)^3 \delta_D(\mathbf{k}+\mathbf{k}') P_{\rm in}(k) = \langle \delta_1 \delta_1 \rangle$. In order to do explicit calculations and check the consistency of the theory, a scale-invariant initial power spectrum is often chosen, thus $P_{\rm in}(k) \propto k^n$ for some n.

2.2 Symmetries

We can learn a lot about our system by investigating which symmetries are satisfied by the equations of motion. Symmetries can help to construct relations among correlation functions, which we can use to check various analytical approaches and also compare them to observations because these relations will be valid at any order in perturbation theory.

Looking at Eqs. 2.3, 2.4, 2.5, specified to an Einstein-de-Sitter universe, $\mathcal{H} = 2/\tau$, it is easy to show that the equations of motion are invariant under SO(3) space rotations and symmetries of the form (following [9])

$$\begin{aligned} &\tau' = \tau, \quad \mathbf{x}' = \mathbf{x} + \mathbf{n}(\tau) \\ &\delta'(\mathbf{x},\tau) = \delta(\mathbf{x}',\tau') \\ &\mathbf{v}'(\mathbf{x},\tau) = \mathbf{v}(\mathbf{x}',\tau') - \dot{\mathbf{n}}(\tau) \\ &\phi'(\mathbf{x},\tau) = \phi(\mathbf{x}',\tau') - \left(\ddot{\mathbf{n}}(\tau) + \frac{2}{\tau} \dot{\mathbf{n}}(\tau) \right) \cdot \mathbf{x}. \end{aligned} \tag{2.10}$$

This symmetry has three important special cases, namely translations, Galilean boosts and acceleration transformations. Translations arise by simply picking an arbitrary constant three-dimensional vector

$\mathbf{n}(\tau) = \mathbf{n}$. This reflects the assumption of homogeneity of the universe. Galilean boosts arise when we choose $\mathbf{n}(\tau) = \mathbf{u}\tau$, where $\mathbf{u}$ is constant. Thus, the system is also invariant under a shift to another reference frame which differs from the present frame by a constant velocity.

For acceleration transformations, $\mathbf{n}(\tau) = \frac{1}{2}\mathbf{a}\tau^2$ is chosen, where $\mathbf{a}$ is again an arbitrary constant three-dimensional vector. This represents invariance between two coordinate systems with a relative uniform acceleration. This symmetry allows us to use comoving coordinates, as described in Sec. 1.1.

Furthermore, the fluid equations are invariant under the Lifshitz scaling for a generic weight z,

$$\begin{aligned} \tau' &= \lambda^z \tau, \quad \mathbf{x}' = \lambda \mathbf{x} \\ \delta'(\mathbf{x}, \tau) &= \delta(\mathbf{x}', \tau') \\ \mathbf{v}'(\mathbf{x}, \tau) &= \lambda^{z-1} \mathbf{v}(\mathbf{x}', \tau') \\ \phi'(\mathbf{x}, \tau) &= \lambda^{2(z-1)} \phi(\mathbf{x}', \tau'). \end{aligned} \tag{2.11}$$

In ΛCDM, Galilean boosts and acceleration transformations are still satisfied, but Lifshitz scaling is no longer a symmetry.

Now that we have found these symmetries in the equations of motion, we might wonder what their physical consequences are. As mentioned in the previous chapter, Sec. 1.3.1, the initial conditions in cosmology are most often Gaussian or nearly Gaussian random fields which are statistically homogeneous and isotropic. One possible realization is thus not expected to satisfy the symmetries, because symmetries only play a role at the statistical level. This means that when the correlator of a given observable is transformed under a given symmetry, then it should still have the same statistical properties as before the transformation. As a consequence, the correlators satisfy certain identities called Ward identities. One example of such an identity which follows from Lifshitz scaling is

$$\langle \delta(\mathbf{x}_1, \tau) \delta(\mathbf{x}_2, \tau) \rangle = F\left(\frac{\tau}{x_{12}^z} \right), \tag{2.12}$$

where $x_{12} = |\mathbf{x_1} - \mathbf{x}_2|$ and F is a function of only τ / x_{12}^z. Comparing this to the linear behaviour at early times, $\langle \delta\delta \rangle \propto \tau^4 / x_{12}^{3+n}$, it follows that $z = 4/(3+n)$. Lifshitz scaling implies that the system is self-similar, which is described in the next section.

2.2.1 Self-similarity

The equations of motion describing gravitational collapse should obey self-similarity, i.e., the system should looks the same on all scales and we can rescale space and time however we want. The requirement of self-similarity gives a time constraint on the effective terms in the equation of motion and thus on c_s and c_v. For this calculation we followed [8], but using cosmic time t instead of the comoving time τ. The equations of motion can easily be rewritten in terms of t and using the density ρ_l instead of the density contrast δ_l, such that the appropriate scaling of the density can also be found. The equations of motion become

$$\begin{aligned} \dot{\rho}_l + 3H\rho_l + \frac{1}{a}\partial(\rho_l v_l^i) &= 0 \\ \dot{v}_l^i + H v_l^i + \frac{1}{a} v_l^j \partial_j v_l^i + \frac{1}{a}\partial^i \phi_l &= -\frac{1}{a\rho_l} \partial_j [\tau^{ij}]_\Lambda \\ \partial^2 \phi_l &= 4\pi G a^2 (\rho_l - \bar{\rho}), \end{aligned} \tag{2.13}$$

where $H = 2/3t$ in Einstein-de Sitter.

For the moment we neglect the effective terms (i.e., the stress-energy tensor). By substituting a scaled solution of the form

$$\begin{aligned} \tilde{\rho}_l(\mathbf{x}, t) &= \lambda_\rho \rho_l(\tilde{\mathbf{x}}, \tilde{t}) \\ \tilde{v}_l^i(\mathbf{x}, t) &= \lambda_v v_l^i(\tilde{\mathbf{x}}, \tilde{t}) \\ \tilde{\phi}_l(\mathbf{x}, t) &= \lambda_\phi \phi_l(\tilde{\mathbf{x}}, \tilde{t}) \end{aligned} \tag{2.14}$$

where $\tilde{x} = \lambda_x x$ and $\tilde{t} = \lambda_t t$, we see that the equations are invariant under this transformation if

$$\lambda_\rho = \lambda_t^2, \quad \lambda_v = \frac{\lambda_t^{1/3}}{\lambda_x}, \quad \lambda_\phi = \frac{\lambda_t^{2/3}}{\lambda_x^2}, \tag{2.15}$$

where we used that $a \propto t^{2/3}$ in EdS, which gives rise to some extra factors λ_t.

Thus, we can now obtain a new solution for any choice of λ_x and λ_t. However, not all the possible choices correspond to a realization of the same cosmology, i.e., not all solutions have initial conditions sampled from the same power spectrum. If we assume power law initial conditions, thus $\Delta^2_{\text{initial}}(k,t) \propto t^{4/3} k^{n+3}$, then

$$\tilde{\Delta}^2_{\text{initial}}(k,t) = \frac{\lambda_t^{4/3}}{\lambda_x^{n+3}} \Delta^2_{\text{initial}}(k,t) \tag{2.16}$$

thus for $\lambda_x = \lambda_t^{\frac{4}{3(n+3)}}$ the rescaled solutions are just different samples of the same initial power spectrum. Comparing this to the symmetries described above, we see that this is just Lifshitz scaling for $\lambda = \lambda_t^{(4n+8)/(15-3n)}$. We know that the full solution satisfies this scaling symmetry, both at long and short scales, thus the effective terms that we neglected should also satisfy the scaling symmetry. This means that all terms scale according to their dimensions. Using Eq. (2.7), it can be deduced that

$$c_s^2, c_{bv}^2, c_{sv}^2 \propto \frac{\lambda_x^2}{\lambda_t^{4/3}}. \tag{2.17}$$

Or, plugging in the condition for λ_x and λ_t, we obtain

$$c_s^2, c_{bv}^2, c_{sv}^2 \propto t^{\frac{-4-4n}{3(n+3)}}. \tag{2.18}$$

This gives a constraint on the time-dependence of the speed of sound and viscosity in an EdS universe with power law initial conditions.

Furthermore, since $\tilde{\Delta}^2_{\text{initial}} = \Delta^2_{\text{initial}}$, this should also hold at any given time, thus

$$\Delta^2(k,\tau) = \tilde{\Delta}^2(k,\tau) = \Delta^2(k/\lambda^{\frac{4}{n+3}}, \lambda\tau), \tag{2.19}$$

which implies that

$$\Delta^2(k,\tau) = \Delta^2(k/k_{\text{NL}}) \tag{2.20}$$

where k_{NL} is defined as in Eq. 1.33 and $k/k_{\text{NL}} \propto k\tau^{4/(3+n)}$ such that it is invariant under the required scaling. Thus, the power spectrum can only be a function of k/k_{NL} and k_{NL} is the only important scale in our theory. This is also reflected by the Ward identity 2.12.

Chapter 3

Spherical Collapse

Linear inhomogeneities are stretched out by the Hubble flow and their size is proportional to the scale factor. On the other hand, when density perturbations are non-linear, the gravitational field created by the perturbation can lead to a contraction which overwhelms the Hubble expansion. As a result, the inhomogeneity drops out of the Hubble flow, reaches its maximal size and recollapses to form a stable non-linear structure. In the previous chapters, perturbation theory has been used in order to obtain a better understanding of this process. As we have seen, it is very hard to obtain exact solutions for such processes when considering realistic density perturbations. Exact solutions can only be found in a few particular cases that possess certain symmetries. One of these cases is a density perturbation that possesses spherical symmetry. Although this assumption is not very realistic, it can still be very useful to study the solutions in order to obtain a qualitative understanding of the non-linear behaviour of inhomogeneities. Thus, in this chapter we will assume that all matter in the universe is distributed in a spherically symmetric way. We will call this the spherical collapse (SC) approximation. Furthermore, we will work in Lagrangian coordinates, which will be briefly explained below.

Lagrangian coordinates The coordinates that we use most often are Eulerian coordinates $\mathbf{x}$. These coordinates describe fixed points in space. In some cases, especially when describing fluids, another coordinate system is more convenient, namely Lagrangian coordinates $\mathbf{q}$. Lagrangian coordinates are not fixed in space, but instead trace the infinitesimal fluid elements. We label a fluid element by its initial position $\mathbf{q}$. Its actual, Eulerian, position is described by $\mathbf{x}(\mathbf{q}, t)$, where $\mathbf{x}(\mathbf{q}, t_0) = \mathbf{q}$ for some initial time t_0. By using Lagrangian coordinates, we consider what happens to one particular fluid element, instead of fixing on one particular point in space.

3.1 Parametric solutions

In the following we assume that shell-crossing (world lines of various dust shells intersect) does not occur. The equation governing the evolution of a spherical shell of radius R collapsing under its own gravity is given by

$$\frac{d^2R}{dt^2} = -\frac{GM}{R^2} \tag{3.1}$$

where G is Newton's constant and M is the mass inside the shell. R is a Lagrangian coordinate which is comoving with the observer, thus we follow the motion of this particular shell. This equation can be solved in the parametric form (following [10])[1]

$$R = \frac{R_i}{1-\cos\eta_i}(1-\cos\eta), \qquad t = \frac{t_i}{\eta_i - \sin\eta_i}(\eta - \sin\eta), \tag{3.2}$$

[1] We use different initial conditions compared to [10], because we think that it is intuitively more clear this way and we do not need any approximation.

where R_i and t_i refer to the initial radius and initial and time. η is a parameter running between 0 and 2π that parametrizes the evolution of the shell and η_i is its value corresponding to $R(\eta_i) = R(t_i) = R_i$ and $t(\eta_i) = t_i$. This solution describes the evolution of overdense regions. For underdensities, similar solutions exist with hyperbolic functions cosh and sinh instead of cos and sin. In this work, we will only consider overdensities. Plugging the parametric solution back in equation (3.1), we see that the solution is valid if

$$\frac{GMt_i^2}{R_i^3} = \frac{(\eta_i - \sin\eta_i)^2}{(1-\cos\eta_i)^3}, \tag{3.3}$$

thus there are still two independent constants left, as should be the case for a second order differential equation. In Fig. 3.1, the spherical collapse solution is plotted for several different initial overdensities. It can be seen that as the initial overdensity is larger, it collapses faster, and small overdensities never collapse and expand forever under influence of the Hubble rate.

We can now derive an equation for $\delta(\eta)$ from our solution (3.2), using that $\bar{\rho} = \frac{1}{6\pi G t^2}$ in an Einstein-de Sitter universe:

$$\begin{aligned}\delta &= \frac{\rho}{\bar{\rho}} - 1 \\ &= \frac{M}{\frac{4}{3}\pi R^3} \cdot 6\pi G t^2 - 1 \\ &= \frac{9}{2}\frac{(\eta - \sin\eta)^2}{(1-\cos\eta)^3} - 1.\end{aligned} \tag{3.4}$$

There is also another specific solution that corresponds to the case $\eta_i = 0$. This solution is given by

$$R(t) = \left(\frac{9}{2}GM\right)^{1/3}(t-t_0)^{2/3}. \tag{3.5}$$

By plugging this solution back in Eq. 3.1, it follows that it is valid for $GMt_i^2/R_i^3 = 9/2$. Expanding Eq. 3.3 around $\eta_i = 0$, the right hand side becomes $2/9 + \mathcal{O}(\eta_i)$ thus indeed we have found a solution for $\eta_i = 0$. Since this solution has only one integration constant, it is not as general as the solutions found above. For this solution, the relation

$$\dot{R}(t) = \frac{2}{3}\frac{R(t)}{t} \tag{3.6}$$

holds for all t. This solution corresponds to a FLRW universe with $\Omega_m = 1$ that expands forever.

3.2 Virialization

In the above description of spherical collapse, the overdensity eventually collapses into a point, reaching infinite density. This is of course unphysical. In reality, this does not happen because there always exist deviations from perfect spherical symmetry. As a result, the spherical overdensity virializes and forms a stationary spherical object. This happens when the virial theorem is satisfied: $K = -\frac{1}{2}U$, where K and U are respectively the kinetic and potential energy. At maximum radius $R_{\max}$ all energy is potential energy. The mass of a shell of width dr is $dm = \rho 4\pi r^2 dr$ and the mass of the region enclosed by this shell is $M_r = (r/R)^3 M$, thus the change in gravitational potential energy of the shell is

$$dU = -\frac{GM_r}{r}dm. \tag{3.7}$$

This can be easily integrated to give

$$U = -\frac{3GM^2}{5R}, \tag{3.8}$$

thus the total energy is given by $E = -3GM^2/5R_{\max}$. When the region has collapsed to $r = R_{max}/2$, we obtain $U = -6GM^2/5R_{max}$ thus $K = E - U = 3GM^2/5R_{\max} = -\frac{1}{2}U(R_{\max}/2)$, thus we see that at

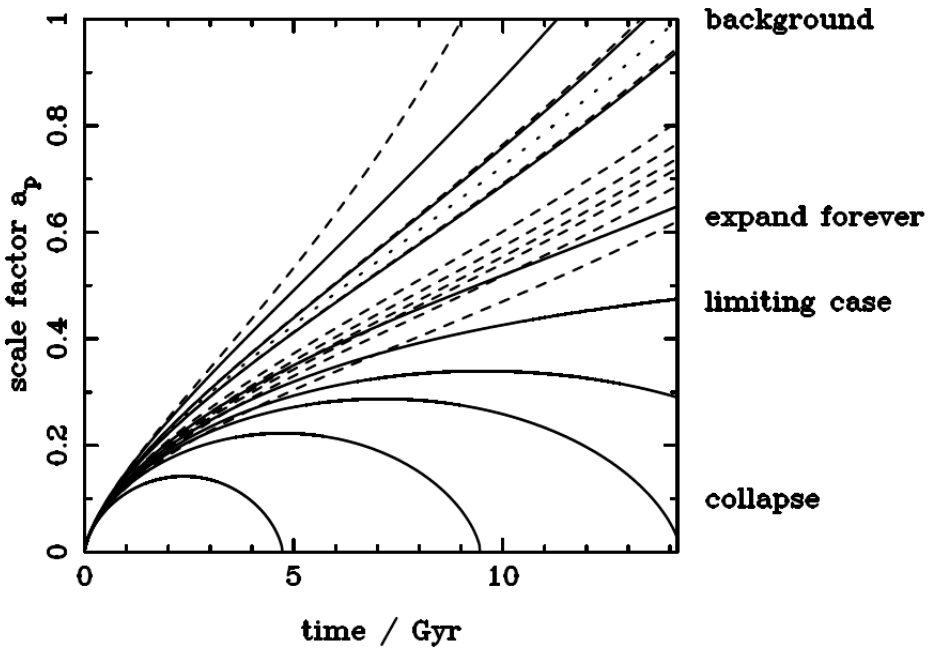

Figure 3.1: Behaviour of overdensities in a ΛCDM-universe with $\Omega_M = 0.25$ for different initial overdensities. Solid lines show the evolution of overdensities in the spherical collapse model, dashed lines show the linear extrapolation of the initial overdensity and the dotted line shows the background expansion. a_p denotes the scale factor of the perturbations, comparable to our radius R [2].

half the maximum radius the virial theorem is satisfied: the system has virialized and became stable. In our parametric solution, the system thus virializes at $\eta = \frac{3\pi}{2}$. This corresponds to $\delta \approx 146$. In order to relate spherical collapse to perturbation theory, we can calculate the value of the linear overdensity $\delta_{\rm lin}$ that corresponds to the moment of virialization. We expand $R(\eta)$ and $t(\eta)$ up to second order around $\eta = 0$ and after some algebra, we obtain

$$\frac{R}{R_{\rm max}} = \frac{1}{4}\left(6\pi\frac{t}{t_{\rm max}}\right)^{2/3}\left[1 - \frac{1}{20}\left(6\pi\frac{t}{t_{\rm max}}\right)^{2/3}\right], \tag{3.9}$$

where $R_{\rm max}$ and $t_{\rm max}$ correspond to $\eta = \pi$ for which the radius of the overdensity is maximal. The first term in this expansion describes the evolution of the background and the second term describes the linear evolution of the perturbation. Furthermore, using that $\rho = \bar{\rho}(1 + \delta_{\rm lin})$, we have

$$1 + \delta_{\rm lin} = \left(\frac{a}{R/R_{\rm max}}\right)^3 \tag{3.10}$$

and it follows that

$$\frac{R/R_{\rm max}}{a} = (1 + \delta_{\rm lin})^{-1/3} \approx 1 - \frac{1}{3}\delta_{\rm lin}. \tag{3.11}$$

Using that $a = \frac{1}{4}(6\pi t/t_{\rm max})^{2/3}$, since this is the first term in Eq. 3.9 which describes the evolution of the background, it follows that

$$\frac{R}{R_{\rm max}} = \frac{1}{4}\left(6\pi\frac{t}{t_{\rm max}}\right)^{2/3}\left(1 - \frac{1}{3}\delta_{\rm lin}\right), \tag{3.12}$$

and comparing this to Eq. 3.9, we obtain

$$\delta_{\text{lin}} = \frac{3}{20}\left(6\pi\frac{t}{t_{\text{max}}}\right)^{2/3}. \tag{3.13}$$

Thus, if we now use the fact that the object virializes at $R = R_{\text{max}}/2$, it follows that $t/t_{\text{max}} = 3/2$ and thus $\delta_{\text{lin}} = 1.392$ [11]. Alternatively, $\eta = 2\pi$ is often taken as the moment of virialization. This results in a slightly different value, namely $\delta_{\text{lin}} = 1.686$. This value corresponds to a non-linear overdensity of approximately 178. Usually, this is used as a rule of thumb that linear theory is correct until the linear overdensity is 1.686 and at that time bound structures with non-linear overdensities of about 178 have suddenly formed [10]. This assumption seems unphysical, but turns out to be a rather good approximation since gravitational instability operates very quickly. Using this method, we can thus interpret the values for δ that are found using linear perturbation theory and relate them to what actually happens in the non-linear regime.

In order to do this, a critical initial density for collapse is defined, which depends on time. At a certain time, perturbations with density larger than this critical density have already collapsed while perturbations with smaller density have not. Usually, this critical initial density is extrapolated to the present, and since it does not dependent strongly on the cosmological model that is used, it can be approximated by its value in EdS,

$$\delta_c \simeq 1.686\frac{D_1(0)}{D_1(a)}, \tag{3.14}$$

where the factor 1.686 was calculated above using spherical collapse and D_1 denotes the linear growth factor, which is equal to a in EdS. δ_c is called the linearly-extrapolated critical density for collapse. This critical density will be imprinted in the large-scale structure and is thus an important quantity to measure.

3.3 Self-similarity in spherical collapse

Following the reasoning of Sec. 2.2.1, the spherically symmetric solutions should also obey self-similarity. Instead of starting from the equations for the density and velocity, equivalently, we can also start with the Newtonian equation of motion,

$$\ddot{R}(q,t) = -\frac{M(R_i)G}{R(R_i,t)^2}, \tag{3.15}$$

where R_i is a radial Lagrangian coordinate representing a particular spherical shell, $M(R_i)$ is the mass in this shell and $R(R_i,t)$ is the position of a particle, with the initial condition $R(R_i,t_i) = R_i$. In order to check whether this equation also obeys self-similarity we plug in a solution $\tilde{R}(R_i,t) \equiv \lambda_R R(\lambda_{R_i}R_i, \lambda_t t)$. It can easily be seen that self-similarity is satisfied if and only if

$$\frac{M(R_i/\lambda_{R_i})}{M(R_i)} = \lambda_t^2\lambda_R^3. \tag{3.16}$$

This implies that $M(R_i/\lambda_{R_i}) = M(R_i)\lambda_{R_i}^{\alpha}$ and $\lambda_R = \lambda_t^{-2/3}\lambda_{R_i}^{\alpha/3}$ for some parameter α.

Now, we would like to relate this α to the n of the power spectrum $P(k) \propto k^n$, since they both have something to do with the initial conditions of the distribution of matter of a self-similar theory. Since the rescaling should be the same for all distances, λ_R and λ_{R_i} should be equal. Otherwise, $R(R_i,t_i) = R_i$ does not hold after rescaling. From this, it follows that

$$\lambda_R^{\alpha-3} = \lambda_t^2, \tag{3.17}$$

and using the relation between λ_x and λ_t found in Sec. 2.2.1, it follows that also $\lambda_R = \lambda_t^{4/(3n+9)}$, thus we obtain

$$\alpha = \frac{15+3n}{2}. \tag{3.18}$$

Chapter 4

Past and Future Experiments

As described in the introduction, large-scale structure surveys have grown significantly over the past years and will likely become the next leading cosmological observable. There is a lot of still unexploited information that can help us to answer questions about inflation, dark energy, dark matter, neutrinos, and so on. Furthermore, observations can confirm predictions made by the EFToLSS and help to determine the values of the effective parameters.

In this chapter, first we will explain how redshift surveys can be used to measure large-scale structures, hereby following [2], and then we will reviewe a couple of experiments from the past and some experiments that are planned for the future.

4.1 The galaxy distribution

The experiments that are being conducted to obtain properties of the large-scale structure of the universe are mostly redshift surveys. In these surveys, the redshift of all luminous objects in a selected region of the sky is measured. Then, the brightness of the objects is used to distinguish between stars and galaxies. Since galaxies are very bright, these are the extragalactic objects that are most often observed in surveys. The redshift data can be combined with angular position data to obtain a three-dimensional distribution of galaxies. In order to obtain as much of the three-dimensional information as possible through the galaxy surveys, a couple of things need to be taken into account. Angular distances can be measured directly and are thus easy to obtain, radial distances on the other hand are much harder and have to be obtained through the redshift data. First, the spectrum of light is measured. This spectrum is used to calculate the redshift of the galaxies and then estimate their distances using the Hubble expansion rate. Furthermore, as will be described in Sec. 4.1.3, when measuring redshift, an effect called redshift-space distortion has to be taken into account to make the data more accurate. In order to further improve the accuracy of both the angular and radial distances, a method using baryon acoustic oscillations can be used. This will be described in Sec. 4.1.2.

Once we have the galaxy distribution, we can extract many interesting statistical properties of the large-scale structure from it, for example the matter density contrast and power spectrum. In order to obtain these properties, first, the matter distribution needs to be deduced from the galaxy distribution. How to do this is described in the next section.

4.1.1 From galaxy distribution to matter distribution

Galaxies are expected to be found at certain special locations in the matter density field, as described by the correlation function, see Sec. 1.3. Let δ_g be the overdensity field of the galaxies and let δ_M be the overdensity field of all matter. Observed galaxies will form a Poisson sample of δ_g, which is not necessarily the same as δ_M. The difference between these two fields is called "bias" and is denoted

by b. The bias encodes the physics of galaxy formation. On large scales it becomes a local, linear function, $b = \delta_g/\delta_M$.

Furthermore, obviously not *all* galaxies in the universe have been measured in a particular survey. In order to correct for this, a so-called survey mask is used, which describes where galaxies could have been observed and not just where they were actually observed [2]. This mask can be split up into a radial and an angular component. The angular component takes care of purity and varying completeness of the observations, while the radial component takes into account the criteria (such as brightness) on the basis of which the galaxies are selected. With the help of this mask, the goal is to obtain a distribution of galaxies that is as complete and trustworthy as possible. Then, it can be translated into the overdensity field. From the Fourier transform of this field, the isotropically averaged power spectrum can be calculated.

The power spectrum and correlation function are all we need to describe the large-scale structures. Namely, as we have seen in the previous chapters, the density contrast $\delta(\mathbf{x})$ describes fluctuations in the density distribution of collisionless dark matter particles. At early times or on large scales, the distribution of $\delta(\mathbf{x})$ is close to Gaussian with adiabatic fluctuations. This means that the statistical distribution can be completely determined by two-point functions $\xi(\mathbf{x}_1, \mathbf{x}_2) \equiv \langle \delta(\mathbf{x}_1)\delta(\mathbf{x}_2)\rangle$, because every higher-order correlator can be rewritten as a product of two-point functions by using Wick's theorem. As mentioned in Ch. 1, statistical homogeneity and isotropy imply that ξ only depends on $|\mathbf{x}_1 - \mathbf{x}_2|$. The fact that the fluctuations are adiabatic means that the overdensity field is equal for all forms of matter and energy.

4.1.2 Baryon acoustic oscillations

One of the hardest parts of interpreting galaxy surveys is to be able to extract cosmic distances from the measurements. To make this a bit easier, the method of baryon acoustic oscillations is used.

In the same way that supernovae are used as standard candles to measure distances and map the cosmological expansion history because they have a known luminosity, there is also a 'standard ruler' encoded in the clustering of galaxies [12]. Namely, it was discovered that pairs of galaxies have a preference for being separated by a comoving distance of 150 Mpc. The separation can be explained by going back to the primordial universe. Before the epoch of last-scattering which produced the CMB, radiation was still the dominant component of the universe. In overdense regions containing dark matter, photons and baryons, there was thus a lot of radiation pressure, causing the launch of spherical wavefronts. These sound waves were able to cover a distance of about 150 Mpc between the big bang and the last-scattering epoch, travelling at a speed of the order $0.58c$. Afterwards, both the initial overdense regions and the spherical baryonic shells around it seeded the formation of galaxies. This resulted in the imprinting of the standard ruler of 150 Mpc in the large-scale clustering pattern. The fluctuations in the density pattern are also called baryon acoustic oscillations, which is often abbreviated as BAO. See Fig. 4.1 for an illustration of this effect.

The standard ruler can be used to improve galaxy surveys both in the radial and in the angular direction. Radially, a preferred redshift-space clustering scale can be calculated, and in the angular direction, a preferred angular clustering scale of approximately 3 degrees is found. These can both be used to determine cosmic distance. The discovery of baryon acoustic oscillations has boosted the power of galaxy redshift surveys significantly.

4.1.3 Redshift-space distortions

Redshift-space distortions are an observational effect that results from the fact that we measure galaxy distances using redshifts. The measured redshift is mostly caused by the Hubble expansion, but also partly by any additional motion of the galaxy under consideration, called the peculiar velocity. Sine we do not know the peculiar velocities of all galaxies, this causes distortions in the measured field. These are called redshift-space distortions (RSD). One source that causes movement of galaxies is the growth of overdensities. Galaxies will move relative to the Hubble flow because they are gravitationally

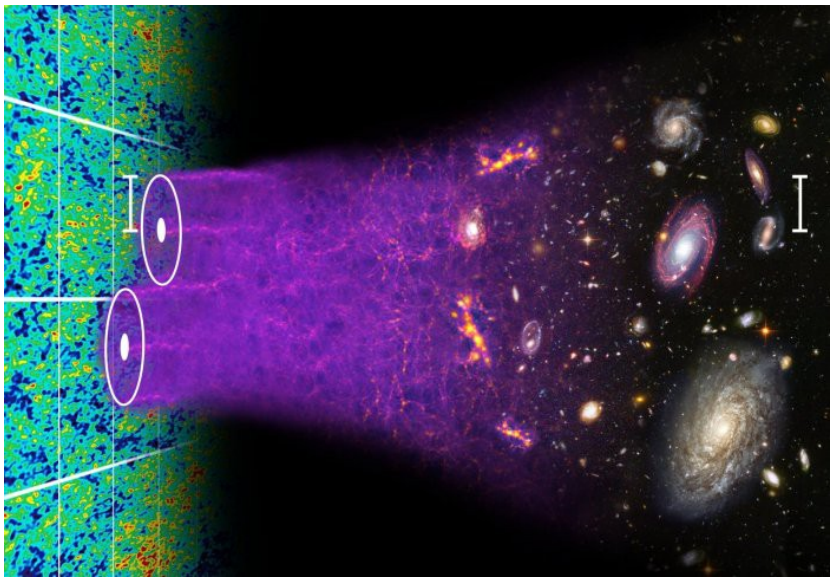

Figure 4.1: Illustration of the concept of baryon acoustic oscillations [13]

attracted to overdensities and repelled by underdensities. On large scales, this is the dominant source of RSD. This effect makes overdense regions appear "squashed" and underdense regions "stretched" along the line of sight, since their peculiar velocity is not taken into account in our model. On small scales, this effect is also present within collapsed objects, resulting in structures pointing towards the observer, called "Fingers of God". If redshift-space distortions are taken into account to correct the data, the accuracy of redshift surveys improves further.

4.2 Past experiments

Many experiments and especially redshift surveys have been done over the course of the years, aiming to give a better understanding of the large-scale structures. In this section we will consider a few of the most important ones.

2dF

2dF is a galaxy redshift survey in which 230 000 galaxies were measured, performed by the Anglo-Australian Observatory (AAO) in 1997-2002. In this survey, the large-scale structure in two large slices around the north and south galactic poles has been determined to a depth of 2.5 billion light years, corresponding to $z \sim 0.2$. The covered volume was of the order 10^8 h^{-1} Mpc^3.

The most important results of 2dF are the measurement of the density parameter of nonrelativistic matter (baryonic matter, dark matter and massive neutrinos), the detection of the baryon acoustic oscillations and a limit on the contribution of neutrinos to dark matter [14].

WiggleZ

WiggleZ is another galaxy redshift survey, performed by the Anglo-Australian Telescope (AAT) between 2006 and 2011, in which the redshift for 240 000 galaxies over 1000 square degrees was measured to a depth of 8 billion light years ($0.2 < z < 1$). This survey aimed to learn more about dark energy through two different methods: measurements of the cosmic distance using the BAO standard ruler technique and measurements of the growth of structure using redshift-space distortions. WiggleZ has

measured a wider redshift range than previous surveys, which resulted in more accurate measurements [12].

SDSS

The Sloan Digital Sky Survey (SDSS) is a redshift survey performed in New Mexico, United States that started in 2000 and has already finished several projects. It is also still collecting data. Between 2000 and 2008, it has mapped more than 8000 square degrees of the sky containing more than one million galaxies. Also, SDSS-II discovered hundreds of supernovae which can be used to measure the expansion history of the universe. Furthermore, BOSS (Baryon Oscillation Spectroscopic Survey, part of SDSS-III) mapped the spatial distribution of about 1.5 million luminous red galaxies for a redshift $z < 0.7$ in order to determine the BAO standard ruler more precisely [13].

4.3 Ongoing experiments

KiloDegree Survey

KiloDegree Survey (KiDS) is a survey that started in 2011 and is mapping 1500 square degrees with median redshift $z \sim 0.7$, partly overlapping with previous surveys such as 2dF and SDSS. The mapped survey area is much smaller than the one in SDSS, but the measurements are more sensitive and the image quality is better [15].

eBOSS

eBOSS (where the e stands for extended) is the next survey done by SDSS. This survey started in 2014 and will go on until 2020. It aims to find galaxies around $z \sim 1$ that were missed by BOSS [13]).

4.4 Future experiments

Euclid

Euclid is a space mission by ESA, which is planned to launch its satellite in 2020. It aims to give an explanation for dark energy and the accelerated expansion of the universe using two methods, namely weak gravitational lensing and galaxy clustering. Weak gravitational lensing is a method to measure masses of astronomical objects which uses the bending of light under the influence of gravity and redshift-space distortion. The galaxy clustering method uses baryon acoustic oscillations to learn more about the distribution of galaxies. Using these methods, Euclid aims to map the evolution of the universe over the past 10 billion years, to be able to answer questions about dark energy, dark matter, gravity and the initial conditions of the early universe. It will map 15 000 square degrees of the darkest sky and its data is supposed to be two orders of magnitude better than what is currently available [16].

DESI

The Dark Energy Spectroscopic Instrument (DESI) will be built with very similar goals as the Euclid mission, but this is not a space mission but again a redshift survey with a telescope located in Arizona, USA. It aims to make a three-dimensional map of the universe over more than a third of the sky, measuring over 35 million galaxies and quasars with redshifts in the range $0 < z < 3.5$. It is supposed to have the world's most powerful wide-field spectograph for wide-field galaxy surveys and be able to obtain thousands of spectra simultaneously. It is planned to start operating in 2019 [17].

4.4.1 Outlook

Over the course of time, a general development can be seen in all of these experiments: more and more galaxies and a larger and larger part of the sky are being mapped. As described in the beginning of this chapter, these experiments can for example help us to obtain more accurate values for the overdensity field and the dark matter distribution. However, the statistical errors still have to be reduced significantly in order to obtain measurements that are precise enough for our goals. Thus, there still remains a lot to be done and all aspects of the analysis need to be checked for potential errors. An example is shown in Fig. 4.2, where the statistical errors of distance measurements using BAO in past measurements and a prediction for those in future measurements are plotted. If the required accuracy is achieved, then future surveys can certainly give us great new insight in the evolution of the universe and can help us to provide answers to the fundamental questions written in the introduction of this thesis.

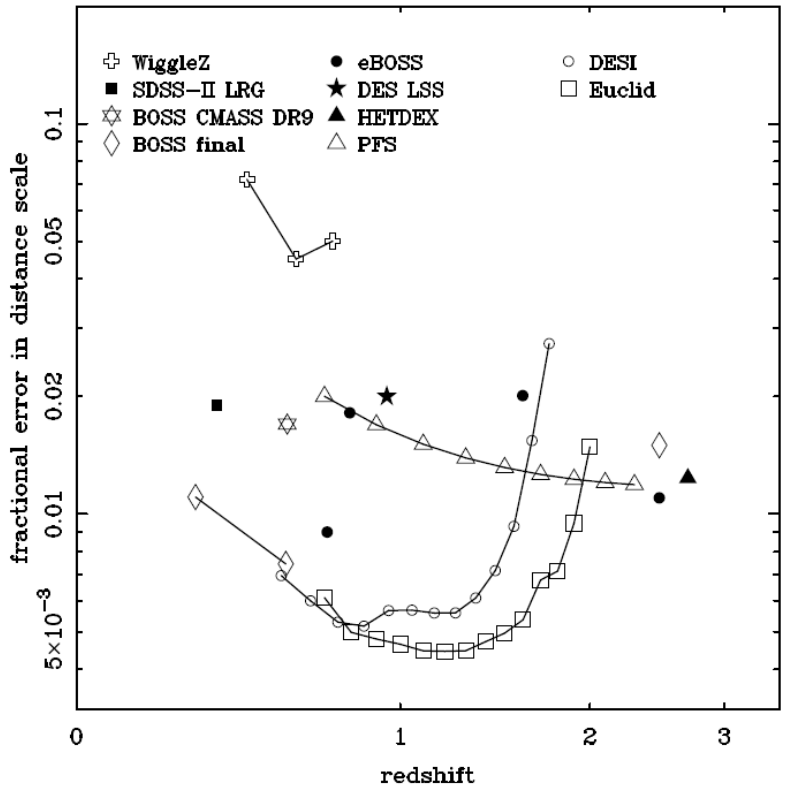

Figure 4.2: Prediction for statistical errors in future BAO measurements [2]

Part II

Calculations

Chapter 5

Calculation of c_s^2 using PT

The goal of this chapter is to find an expression for the effective parameter $c^2_{\rm comb} = c_s^2 + c_v^2$ by using the perturbative approach of EFToLSS. In standard perturbation theory, we can expand $\delta = \delta_1 + \delta_2 + \delta_3 + \dots$. However, when we calculate the power spectrum using this expansion, some of the terms contain divergent loop integrals. In the EFToLSS, new terms appear which exactly cancel these divergences. The UV-divergent part of P_{13} should be cancelled by the UV-divergent part of $P_{c_s^2}$, where $P_{c_s^2}$ is the contribution to the power spectrum coming from the speed of sound and viscosity. Thus, we will calculate δ_3 and then require that $\delta_{c_s^2}$ exactly cancels its divergent part to be able to obtain an expression for $c^2_{\rm comb}$. In order to do this, we will first combine the equations of motion into one fluid equation and then expand the right hand side of this equation up to third order in perturbation theory.

Combining Eqs. (1.11) and (1.12), we can find one equation for δ by solving θ from (1.11) and plugging it into (1.12). Afterwards, we rewrite the derivatives using the chain rule to obtain derivatives with respect to the scale factor a. This gives the following equation in Fourier space

$$\begin{aligned}\Box\delta &\equiv -a^2\mathcal{H}^2\delta'' - \frac{3}{2}a\mathcal{H}^2\delta' + \frac{3}{2}\mathcal{H}^2\delta \\ &= -\int_{\mathbf{q}} \beta(\mathbf{q},\mathbf{k}-\mathbf{q})\theta(\mathbf{q})\theta(\mathbf{k}-\mathbf{q}) + \mathcal{H}\partial_a\left(a\int_{\mathbf{q}}\alpha(\mathbf{q},\mathbf{k}-\mathbf{q})\delta(\mathbf{k}-\mathbf{q})\theta(\mathbf{q})\right),\end{aligned} \tag{5.1}$$

where a prime denotes a derivative with respect to a.

5.1 Third order perturbation theory

Up to third order, the fluid equation becomes

$$\begin{aligned}\Box\delta_3 &= -2\int_{\mathbf{q}}\beta(\mathbf{q},\mathbf{k}-\mathbf{q})\theta_1(\mathbf{q})\theta_2(\mathbf{k}-\mathbf{q}) + \mathcal{H}\partial_a\left(a\int_{\mathbf{q}}\alpha(\mathbf{q},\mathbf{k}-\mathbf{q})\left[\delta_1(\mathbf{k}-\mathbf{q})\theta_2(\mathbf{q}) + \delta_2(\mathbf{k}-\mathbf{q})\theta_1(\mathbf{q})\right]\right) \\ &= -2\mathcal{H}^2a^3\int_{\mathbf{q},\mathbf{q_1},\mathbf{q_2}}\beta(\mathbf{q},\mathbf{k}-\mathbf{q})\delta_D(\mathbf{k}-\mathbf{q}-\mathbf{q_1}-\mathbf{q_2})G_2(\mathbf{q_1},\mathbf{q_2})\delta_1(\mathbf{q})\delta_1(\mathbf{q_1})\delta_1(\mathbf{q_2}) \\ &\quad - \mathcal{H}\partial_a\Big(a^{7/2}\mathcal{H}_0\int_{\mathbf{q},\mathbf{q_1},\mathbf{q_2}}\alpha(\mathbf{q},\mathbf{k}-\mathbf{q})\big[\delta_D(\mathbf{q}-\mathbf{q_1}-\mathbf{q_2})G_2(\mathbf{q_1},\mathbf{q_2})\delta_1(\mathbf{k}-\mathbf{q})\delta_1(\mathbf{q_1})\delta_1(\mathbf{q_2}) \\ &\qquad\qquad + \delta_D(\mathbf{k}-\mathbf{q}-\mathbf{q_1}-\mathbf{q_2})F_2(\mathbf{q_1},\mathbf{q_2})\delta_1(\mathbf{q})\delta_1(\mathbf{q_1})\delta_1(\mathbf{q_2})\big]\Big),\end{aligned}$$

where we used Eqs. (1.15) and (1.16) for the first and second order expressions, namely

$$\begin{aligned}\theta_1(\mathbf{q}) &= -a\mathcal{H}\delta_1(\mathbf{q})\\ \theta_2(\mathbf{q}) &= -a^2\mathcal{H}\int_{\mathbf{q_1}}\int_{\mathbf{q_2}}\delta_D(\mathbf{q}-\mathbf{q_1}-\mathbf{q_2})G_2(\mathbf{q_1},\mathbf{q_2})\delta_1(\mathbf{q_1})\delta_1(\mathbf{q_2})\\ \delta_2(\mathbf{q}) &= a^2\int_{\mathbf{q_1}}\int_{\mathbf{q_2}}\delta_D(\mathbf{q}-\mathbf{q_1}-\mathbf{q_2})F_2(\mathbf{q_1},\mathbf{q_2})\delta_1(\mathbf{q_1})\delta_1(\mathbf{q_2}).\end{aligned} \tag{5.2}$$

Note that the kernels F_2 and G_2 are now actually the symmetrized kernels, but we dropped the superscript for notational convenience. Using $\mathcal{H} = \mathcal{H}_0/a$ to perform the derivative with respect to a gives

$$\begin{aligned}\Box\delta_3 &= -2a^2\mathcal{H}_0^2\int_{\mathbf{q},\mathbf{q_1},\mathbf{q_2}}\beta(\mathbf{q},\mathbf{k}-\mathbf{q})\delta_D(\mathbf{k}-\mathbf{q}-\mathbf{q_1}-\mathbf{q_2})G_2(\mathbf{q_1},\mathbf{q_2})\delta_1(\mathbf{q})\delta_1(\mathbf{q_1})\delta_1(\mathbf{q_2})\\ &\quad -\frac{7}{2}a^2\mathcal{H}_0^2\int_{\mathbf{q},\mathbf{q_1},\mathbf{q_2}}\delta_1(\mathbf{q})\delta_1(\mathbf{q_1})\delta_1(\mathbf{q_2})\delta_D(\mathbf{k}-\mathbf{q}-\mathbf{q_1}-\mathbf{q_2})\\ &\qquad\qquad\big[\alpha(\mathbf{k}-\mathbf{q},\mathbf{q})G_2(\mathbf{q_1},\mathbf{q_2})+\alpha(\mathbf{q},\mathbf{k}-\mathbf{q})F_2(\mathbf{q_1},\mathbf{q_2})\big]\\ &= -a^2\mathcal{H}_0^2\int_{\mathbf{q},\mathbf{q_1},\mathbf{q_2}}\delta_D(\mathbf{k}-\mathbf{q}-\mathbf{q_1}-\mathbf{q_2})\delta_1(\mathbf{q})\delta_1(\mathbf{q_1})\delta_1(\mathbf{q_2})\\ &\qquad\qquad\Big\{2\beta(\mathbf{q},\mathbf{k}-\mathbf{q})G_2(\mathbf{q_1},\mathbf{q_2})+\frac{7}{2}\big[\alpha(\mathbf{k}-\mathbf{q},\mathbf{q})G_2(\mathbf{q_1},\mathbf{q_2})+\alpha(\mathbf{q},\mathbf{k}-\mathbf{q})F_2(\mathbf{q_1},\mathbf{q_2})\big]\Big\}\\ &= -9a^2\mathcal{H}_0^2\int_{\mathbf{q},\mathbf{q_1}}\delta_1(\mathbf{q})\delta_1(\mathbf{q_1})\delta_1(\mathbf{k}-\mathbf{q}-\mathbf{q_1})\Big\{\frac{2}{9}\beta(\mathbf{q},\mathbf{k}-\mathbf{q})G_2(\mathbf{q_1},\mathbf{k}-\mathbf{q}-\mathbf{q_1})\\ &\qquad\qquad+\frac{7}{18}\big[\alpha(\mathbf{k}-\mathbf{q},\mathbf{q})G_2(\mathbf{q_1},\mathbf{k}-\mathbf{q}-\mathbf{q_1})+\alpha(\mathbf{q},\mathbf{k}-\mathbf{q})F_2(\mathbf{q_1},\mathbf{k}-\mathbf{q}-\mathbf{q_1})\big]\Big\},\end{aligned}$$

where we used the δ_D-function to perform the integral over q_2 in the last step. Now, we rename the integration variables $q = \tilde{q}_1$ and $q_1 = \tilde{q}_3$ and introduce $\tilde{q}_2 = k - \tilde{q}_1 - \tilde{q}_3$ in the step afterwards.

$$\begin{aligned}\Box\delta_3 &= -9a^2\mathcal{H}_0^2\int_{\tilde{\mathbf{q}}_1,\tilde{\mathbf{q}}_3}\delta_1(\tilde{\mathbf{q}}_1)\delta_1(\tilde{\mathbf{q}}_3)\delta_1(\mathbf{k}-\tilde{\mathbf{q}}_1-\tilde{\mathbf{q}}_3)\Big\{\frac{2}{9}\beta(\tilde{\mathbf{q}}_1,\mathbf{k}-\tilde{\mathbf{q}}_1)G_2(\tilde{\mathbf{q}}_3,\mathbf{k}-\tilde{\mathbf{q}}_1-\tilde{\mathbf{q}}_3)\\ &\qquad\qquad+\frac{7}{18}\big[\alpha(\mathbf{k}-\tilde{\mathbf{q}}_1,\tilde{\mathbf{q}}_1)G_2(\tilde{\mathbf{q}}_3,\mathbf{k}-\tilde{\mathbf{q}}_1-\tilde{\mathbf{q}}_3)+\alpha(\tilde{\mathbf{q}}_1,\mathbf{k}-\tilde{\mathbf{q}}_1)F_2(\tilde{\mathbf{q}}_3,\mathbf{k}-\tilde{\mathbf{q}}_1-\tilde{\mathbf{q}}_3)\big]\Big\}\\ &= -9a^2\mathcal{H}_0^2\int_{\tilde{\mathbf{q}}_1,\tilde{\mathbf{q}}_3}\delta_1(\tilde{\mathbf{q}}_1)\delta_1(\tilde{\mathbf{q}}_2)\delta_1(\tilde{\mathbf{q}}_3)\\ &\qquad\Big\{\frac{2}{9}\beta(\tilde{\mathbf{q}}_1,\tilde{\mathbf{q}}_2+\tilde{\mathbf{q}}_3)G_2(\tilde{\mathbf{q}}_3,\tilde{\mathbf{q}}_2)+\frac{7}{18}\big[\alpha(\tilde{\mathbf{q}}_2+\tilde{\mathbf{q}}_3,\tilde{\mathbf{q}}_1)G_2(\tilde{\mathbf{q}}_3,\tilde{\mathbf{q}}_2)+\alpha(\tilde{\mathbf{q}}_1,\tilde{\mathbf{q}}_2+\tilde{\mathbf{q}}_3)F_2(\tilde{\mathbf{q}}_3,\tilde{\mathbf{q}}_2)\big]\Big\}.\end{aligned}$$

Using that β, G_2 and F_2 are symmetric in their arguments and then in half of the terms switching $\tilde{q}_1$ and $\tilde{q}_3$, we can rewrite the expression within curly brackets,

$$\begin{aligned}\Box\delta_3 &= -9a^2\mathcal{H}_0^2\int_{\tilde{\mathbf{q}}_1,\tilde{\mathbf{q}}_3}\delta_1(\tilde{\mathbf{q}}_1)\delta_1(\tilde{\mathbf{q}}_2)\delta_1(\tilde{\mathbf{q}}_3)\\ &\qquad\Big\{\frac{1}{9}\beta(\tilde{\mathbf{q}}_1,\tilde{\mathbf{q}}_2+\tilde{\mathbf{q}}_3)G_2(\tilde{\mathbf{q}}_2,\tilde{\mathbf{q}}_3)+\frac{1}{9}\beta(\tilde{\mathbf{q}}_2+\tilde{\mathbf{q}}_3,\tilde{\mathbf{q}}_1)G_2(\tilde{\mathbf{q}}_3,\tilde{\mathbf{q}}_2)\\ &\qquad\quad+\frac{7}{18}\alpha(\tilde{\mathbf{q}}_2+\tilde{\mathbf{q}}_3,\tilde{\mathbf{q}}_1)G_2(\tilde{\mathbf{q}}_3,\tilde{\mathbf{q}}_2)+\frac{7}{18}\alpha(\tilde{\mathbf{q}}_1,\tilde{\mathbf{q}}_2+\tilde{\mathbf{q}}_3)F_2(\tilde{\mathbf{q}}_2,\tilde{\mathbf{q}}_3)\Big\}\\ &= -9a^2\mathcal{H}_0^2\int_{\tilde{\mathbf{q}}_1,\tilde{\mathbf{q}}_3}\delta_1(\tilde{\mathbf{q}}_1)\delta_1(\tilde{\mathbf{q}}_2)\delta_1(\tilde{\mathbf{q}}_3)\\ &\qquad\Big\{\frac{1}{9}\beta(\tilde{\mathbf{q}}_1,\tilde{\mathbf{q}}_2+\tilde{\mathbf{q}}_3)G_2(\tilde{\mathbf{q}}_2,\tilde{\mathbf{q}}_3)+\frac{1}{9}\beta(\tilde{\mathbf{q}}_1+\tilde{\mathbf{q}}_2,\tilde{\mathbf{q}}_3)G_2(\tilde{\mathbf{q}}_1,\tilde{\mathbf{q}}_2)\\ &\qquad\quad+\frac{7}{18}\alpha(\tilde{\mathbf{q}}_1+\tilde{\mathbf{q}}_2,\tilde{\mathbf{q}}_3)G_2(\tilde{\mathbf{q}}_1,\tilde{\mathbf{q}}_2)+\frac{7}{18}\alpha(\tilde{\mathbf{q}}_1,\tilde{\mathbf{q}}_2+\tilde{\mathbf{q}}_3)F_2(\tilde{\mathbf{q}}_2,\tilde{\mathbf{q}}_3)\Big\}\end{aligned}$$

such that we can plug in F_3, using the recursion relation (1.17) and symmetrizing,

$$\begin{aligned} F_3(\mathbf{q_1},\mathbf{q_2},\mathbf{q_3}) = \frac{1}{9}\beta(\mathbf{q_1},\mathbf{q_2}+\mathbf{q_3})G_2(\mathbf{q_2},\mathbf{q_3}) + \frac{1}{9}\beta(\mathbf{q_1}+\mathbf{q_2},\mathbf{q_3})G_2(\mathbf{q_1},\mathbf{q_2}) \\ + \frac{7}{18}\alpha(\mathbf{q_1},\mathbf{q_2}+\mathbf{q_3})F_2(\mathbf{q_2},\mathbf{q_3}) + \frac{7}{18}\alpha(\mathbf{q_1}+\mathbf{q_2},\mathbf{q_3})G_2(\mathbf{q_1},\mathbf{q_2}). \end{aligned} \tag{5.3}$$

Finally, we obtain

$$\begin{aligned} \Box\delta_3 &= -9a^2\mathcal{H}_0^2 \int_{\tilde{\mathbf{q}}_1,\tilde{\mathbf{q}}_3} \delta_1(\tilde{\mathbf{q}}_1)\delta_1(\tilde{\mathbf{q}}_2)\delta_1(\tilde{\mathbf{q}}_3)F_3(\tilde{\mathbf{q}}_1,\tilde{\mathbf{q}}_2,\tilde{\mathbf{q}}_3) \\ &= -9a^2\mathcal{H}_0^2 \int_{\mathbf{q},\mathbf{q}_1} \delta_1(\mathbf{q})\delta_1(\mathbf{k}-\mathbf{q}-\mathbf{q}_1)\delta_1(\mathbf{q}_1)F_3(\mathbf{q},\mathbf{k}-\mathbf{q}-\mathbf{q}_1,\mathbf{q}_1), \end{aligned} \tag{5.4}$$

where we switched back to our old variables in the last step.

Now we want to take the expectation value of $\Box\delta_3$ over the short modes, because eventually we want to compare it to $\delta_{c_s^2}$, which appears after averaging out the short modes (see Ch. 2).
In our expression for $\Box\delta_3$, there are three first order perturbations. Each of these can be a short or a long mode. Since we want to describe the net effect of short modes on long modes, and this effect arises when two short modes couple to form one long mode, we will need at least two of the three perturbations to be short. Three short modes will contribute to the stochastic term $\Delta\tau^{ij}$. The term we are looking for thus consists of two short modes and one long mode [18],

$$\begin{aligned} \langle\Box\delta_3\rangle_s &= -9a^2\mathcal{H}_0^2 \int_{\mathbf{q},\mathbf{q_1}} \Big[\langle\delta_1(\mathbf{q})\delta_1(\mathbf{q_1})\rangle_s\delta_1(\mathbf{k}-\mathbf{q}-\mathbf{q_1}) + \langle\delta_1(\mathbf{q})\delta_1(\mathbf{k}-\mathbf{q}-\mathbf{q_1})\rangle_s\delta_1(\mathbf{q_1}) \\ &\qquad + \langle\delta_1(\mathbf{q_1})\delta_1(\mathbf{k}-\mathbf{q}-\mathbf{q_1})\rangle_s\delta_1(\mathbf{q})\Big]2F_3(\mathbf{q},\mathbf{k}-\mathbf{q}-\mathbf{q_1},\mathbf{q_1}) \\ &= -9a^2\mathcal{H}_0^2 \int_{\mathbf{q},\mathbf{q_1}} (2\pi)^3\Big[\delta_D(\mathbf{q}+\mathbf{q_1})P_\delta(q)\delta_l(\mathbf{k}-\mathbf{q}-\mathbf{q_1}) + \delta_D(\mathbf{k}-\mathbf{q_1})P_\delta(q)\delta_l(\mathbf{q_1}) \\ &\qquad + \delta_D(\mathbf{k}-\mathbf{q})P_\delta(q_1)\delta_l(\mathbf{q})\Big]F_3(\mathbf{q},\mathbf{k}-\mathbf{q}-\mathbf{q_1},\mathbf{q_1}) \\ &= -27a^2\mathcal{H}_0^2 \int_{\mathbf{q}} P_\delta(q)\delta_l(\mathbf{k})F_3(\mathbf{q},\mathbf{k},-\mathbf{q}) \\ &= -27a^2\mathcal{H}_0^2\delta_l(\mathbf{k}) \int_{\mathbf{q}} P_\delta(q)F_3(\mathbf{k},\mathbf{q},-\mathbf{q}), \end{aligned}$$

where we used that $\langle\delta_1(\mathbf{q}_1)\delta_1(\mathbf{q}_2)\rangle = (2\pi)^3\delta_D(\mathbf{q}_1+\mathbf{q}_2)P_\delta(q_1)$. Because we assumed that $\delta_l(\mathbf{k})$ is a long mode, we have that $k \ll q$, thus we want to expand F_3 for small k. Using Eq. 5.3, we can straightforwardly obtain an explicit expression for $F_3^{(s)}(\mathbf{k},\mathbf{q},-\mathbf{q})$ which we then expand,

$$\begin{aligned} \langle\Box\delta_3\rangle_s &= -27a^2\mathcal{H}_0^2\delta_l(\mathbf{k}) \int_{\mathbf{q}} P_\delta(q)\Bigg\{\frac{1}{|\mathbf{k}-\mathbf{q}|^2}\left[\frac{5k^2}{126} - \frac{11\mathbf{k}\cdot\mathbf{q}}{108} + \frac{7(\mathbf{k}\cdot\mathbf{q})^2}{108k^2} - \frac{k^2(\mathbf{k}\cdot\mathbf{q})^2}{54q^4} + \frac{4(\mathbf{k}\cdot\mathbf{q})^3}{189q^4}\right. \\ &\quad \left. - \frac{23k^2\mathbf{k}\cdot\mathbf{q}}{756q^2} + \frac{25(\mathbf{k}\cdot\mathbf{q})^2}{252q^2} - \frac{2(\mathbf{k}\cdot\mathbf{q})^3}{27k^2q^2}\right] + \frac{1}{|\mathbf{k}+\mathbf{q}|^2}\left[\frac{5k^2}{126} + \frac{11\mathbf{k}\cdot\mathbf{q}}{108} - \frac{7(\mathbf{k}\cdot\mathbf{q})^2}{108k^2}\right. \\ &\quad \left. - \frac{4k^2(\mathbf{k}\cdot\mathbf{q})^2}{27q^4} - \frac{53(\mathbf{k}\cdot\mathbf{q})^3}{189q^4} + \frac{23k^2\mathbf{k}\cdot\mathbf{q}}{756q^2} - \frac{121(\mathbf{k}\cdot\mathbf{q})^2}{756q^2} - \frac{5(\mathbf{k}\cdot\mathbf{q})^3}{27k^2q^2}\right]\Bigg\} \\ &= -27a^2\mathcal{H}_0^2\delta_l(\mathbf{k})\frac{2\pi}{(2\pi)^3}\int dq\ q^2\int_{-1}^{1} d\mu\ P_\delta(q)\Bigg\{\frac{1}{q^2}\left[1 + \frac{2\mu k}{q} + \frac{(4\mu^2-1)k^2}{q^2} + \mathcal{O}\left(\frac{k^3}{q^3}\right)\right]\cdot \\ &\quad \cdot\left[\frac{5k^2}{126} - \frac{11kq\mu}{108} + \frac{7q^2\mu^2}{108} - \frac{k^4\mu^2}{54q^2} + \frac{4k^3\mu^3}{189q} - \frac{23k^3\mu}{756q} + \frac{25k^2\mu^2}{252} - \frac{2kq\mu^3}{27}\right] \end{aligned}$$

$$+\frac{1}{q^2}\left[1-\frac{2\mu k}{q}+\frac{(4\mu^2-1)k^2}{q^2}+\mathcal{O}\left(\frac{k^3}{q^3}\right)\right]\left[\frac{5k^2}{126}+\frac{11kq\mu}{108}-\frac{7q^2\mu^2}{108}-\frac{4k^4\mu^2}{27q^2}-\frac{53k^3\mu^3}{189q}\right.$$
$$\left.+\frac{23k^3\mu}{756q}-\frac{121k^2\mu^2}{756}-\frac{5kq\mu^3}{27}\right]\Bigg\},$$

where we expanded

$$\frac{1}{|\mathbf{k}\pm\mathbf{q}|^2}=\frac{1}{q^2+k^2\mp 2\mathbf{k}\cdot\mathbf{q}}=\frac{1}{q^2}\left(1\mp\frac{2\mu k}{q}+\frac{(4\mu^2-1)k^2}{q^2}+\mathcal{O}\left(\frac{k^3}{q^3}\right)\right) \tag{5.5}$$

for $k\ll q$ up to third order, using that $\mathbf{k}\cdot\mathbf{q}=kq\cos\theta=kq\mu$. Working out the brackets and performing the angular integral results in

$$\begin{aligned}\langle\Box\delta_3\rangle_s&=-27a^2\mathcal{H}_0^2\delta_l(\mathbf{k})\frac{2\pi}{(2\pi)^3}\int dq\ q^2\int_{-1}^{1}d\mu\ P_\delta(q)\Bigg\{\frac{5}{63}\frac{k^2}{q^2}-\frac{5k^4}{63q^4}+\left(-\frac{59k^2}{126q^2}+\frac{155k^4}{378q^4}+\frac{k^6}{6q^6}\right)\mu^2\\&+\left(-\frac{7k}{27q}+\frac{268k^3}{189q^3}+\frac{14k^5}{27q^5}\right)\mu^3+\left(\frac{2k^2}{9q^2}-\frac{58k^4}{63q^4}-\frac{2k^6}{3q^6}\right)\mu^4+\left(-\frac{28k^3}{27q^3}-\frac{28k^5}{27q^5}\right)\mu^5\Bigg\}\\&=-27a^2\mathcal{H}_0^2\delta_l(\mathbf{k})\frac{2\pi}{(2\pi)^3}\int dq\ P_\delta(q)\left\{-\frac{61}{945}k^2+\frac{128}{2835}\frac{k^4}{q^2}-\frac{7}{45}\frac{k^6}{q^4}\right\}.\end{aligned}$$

Finally, we assume that $P_\delta(q)=Aq^n$ and then perform the integral for the case $n=0$, where k_c is the cut-off wave number that we have to introduce because otherwise the integral diverges. We obtain

$$\begin{aligned}\langle\Box\delta_3\rangle_s&=27Aa^2\mathcal{H}_0^2\delta_l(\mathbf{k})\frac{1}{(2\pi)^2}\frac{61}{945}k^2k_c\\&=\frac{61}{70}\frac{A}{2\pi^2}a^2k^2k_c\mathcal{H}_0^2\delta_l(\mathbf{k}).\end{aligned} \tag{5.6}$$

Using the above calculation, we can now solve the equation

$$\langle\Box\delta_3\rangle_s=-27a^2\mathcal{H}_0^2\delta_l(\mathbf{k})\int_{\mathbf{q}}P_\delta(q)F_3(\mathbf{k},\mathbf{q},-\mathbf{q}) \tag{5.7}$$

by using the retarded Green's function in EdS [8],

$$G(a,\tilde{a})=\frac{2}{5}\mathcal{H}_0^{-2}\theta(a-\tilde{a})\left[\left(\frac{\tilde{a}}{a}\right)^{3/2}-\frac{a}{\tilde{a}}\right], \tag{5.8}$$

to obtain

$$\begin{aligned}\delta_3(\mathbf{k})&=\int d\tilde{a}\ G(a,\tilde{a})\left(-27\tilde{a}^2\mathcal{H}_0^2\delta_l(\mathbf{k})\int_{\mathbf{q}}P_\delta(q)F_3(\mathbf{k},\mathbf{q},-\mathbf{q})\right)\\&=-27\mathcal{H}_0^2\delta_l(\mathbf{k})\int_{\mathbf{q}}P_\delta(q)F_3(\mathbf{k},\mathbf{q},-\mathbf{q})\int d\tilde{a}\ \tilde{a}^2G(a,\tilde{a})\\&=3a^3\delta_l(\mathbf{k})\int_{\mathbf{q}}P_\delta(q)F_3(\mathbf{k},\mathbf{q},-\mathbf{q})\\&=\frac{61}{630}\frac{A}{2\pi^2}a^3k^2k_c\delta_l(\mathbf{k}).\end{aligned} \tag{5.9}$$

We now have an expression for δ_3 for the case $n=0$ and we can calculate $\delta_{c_s^2}$ by using the fact that

$$\Box\delta=c_s^2k^2\delta_l(\mathbf{k})+c_v^2k^2a\partial_a\delta_l(\mathbf{k})-J+\ldots, \tag{5.10}$$

where the terms on the right hand side are the same effective terms mentioned in Ch. 2. δ_{c_s} is then defined as the contribution to δ which takes the effective terms with c_s^2 and c_v^2 into account, thus we can solve the above equation to obtain

$$\begin{aligned}\delta_{c_s^2}(\mathbf{k}) &= \int d\tilde{a}\ G(a,\tilde{a})k^2(c_s^2 + c_v^2 a\partial_a)\delta_1(\mathbf{k}) \\ &= \int d\tilde{a}\ G(a,\tilde{a})k^2(c_s^2 + c_v^2)\delta_l(\mathbf{k}) \\ &= -\frac{1}{9}\mathcal{H}_0^{-2}k^2a^3(c_s^2 + c_v^2)\delta_l(\mathbf{k}),\end{aligned} \tag{5.11}$$

where we performed the integral over $\tilde{a}$ by using that $\delta_l \propto \tilde{a}$ because it is first order in perturbation theory and $c_s^2, c_v^2 \propto \tilde{a}$ because the time-dependences of $\delta_{c_s^2}$ and δ_3 must be equal for their divergent parts to cancel. Thus, if we want the UV-divergent parts of $\delta_{c_s^2}$ and δ_3 to cancel, we need that

$$c_s^2 + c_v^2 = \frac{61}{70}\frac{k_c A\mathcal{H}_0^2}{2\pi^2}. \tag{5.12}$$

This result agrees with an alternative method, where we follow Appendix D from [6]. This method is worked out explicitly in Appendix A.

Note that now we have not found the full $c_s^2 + c_v^2$, but only the divergent part that is needed to cancel the divergent loop integral in P_{13}. The effective parameters also have a finite part that does not depend on the cut-off and can only be determined through simulations or measurements at a specific time. This finite part will act as a renormalization of the theory and its time-dependence is specified by self-similarity as shown in Sec. 2.2.1.

Chapter 6

Calculation of c_s^2 using SC

The goal of this chapter is to obtain an expression for c_s^2 without using perturbation theory. In order to do this, we have to make some simplifying assumptions because we cannot solve the equations of motion exactly. We will assume that gravitational collapse obeys spherical symmetry, and thus that the overdensity has a top-hat shape. Then, we want to find an expression for the non-linear or effective terms in the equation of motion to be able to extract c_s^2.

As we saw in Chapter 3, while using the spherical collapse approximation, δ, t and R can be written in terms of the paramater η as

$$\begin{aligned} \delta &= \frac{9}{2}\frac{(\eta-\sin\eta)^2}{(1-\cos\eta)^3} - 1, \\ R &= \frac{R_i}{1-\cos\eta_i}(1-\cos\eta), \\ t &= \frac{t_i}{\eta_i \sin\eta_i}(\eta-\sin\eta). \end{aligned} \tag{6.1}$$

Now consider the equations of motion in terms of δ, v^i and time t,

$$\begin{aligned} \dot{\delta} + \frac{1}{a}\partial_i((1+\delta)v^i) &= 0 \\ \dot{v}^i + \frac{\dot{a}}{a}v^i + \frac{1}{a}v^j\partial_j v^i + \frac{1}{a}\partial_i\phi &= 0 \\ \nabla^2\phi &= 4\pi G\bar{\rho}a^2\delta, \end{aligned} \tag{6.2}$$

where a dot denotes a derivative with respect to t. We want to rewrite these equations into one equation for δ. Because we initially have a top-hat density distribution which remains top-hat during spherical collapse, we can use $\partial_i\delta = 0$ and $\partial_j\partial_i v^i = \partial_j\theta(t) = 0$. From this, it follows that $v^i = x^i\theta(t)$ thus $\partial_i v^k = \frac{1}{3}\delta_i^k\theta(t)$ and $\partial_i v^k\partial_k v^i = \frac{1}{9}\delta_i^k\delta_k^i\theta(t)^2 = \frac{1}{3}\theta^2$. Using this, we will rewrite the equations of motion. From the continuity equation, it follows that

$$\theta = -\frac{a\dot{\delta}}{1+\delta}. \tag{6.3}$$

For the Euler equation, we take the derivative with respect to x^i on both sides, which results in

$$\begin{aligned} 0 &= \dot{\theta} + \frac{\dot{a}}{a}\theta + \frac{1}{a}\partial_i v^j\partial_j v^i + \frac{1}{a}v^j\partial_j\theta + \frac{1}{a}\nabla^2\phi \\ &= \dot{\theta} + \frac{\dot{a}}{a}\theta + \frac{1}{3a}\theta^2 + 4\pi G\bar{\rho}a\delta. \end{aligned} \tag{6.4}$$

Taking the derivative of (6.3) with respect to t and plugging $\dot{\theta}$ and θ into the Euler equation results in one equation for δ:

$$\ddot{\delta} + \frac{2\dot{a}}{a}\dot{\delta} - \frac{4}{3}\frac{\dot{\delta}^2}{1+\delta} - 4\pi G\bar{\rho}\delta(1+\delta) = 0, \tag{6.5}$$

so putting all non-linear terms on the right hand side, we obtain

$$\ddot{\delta} + \frac{2\dot{a}}{a}\dot{\delta} - \frac{2}{3t^2}\delta = \frac{4}{3}\frac{\dot{\delta}^2}{1+\delta} + \frac{2}{3t^2}\delta^2, \tag{6.6}$$

where in the last step we used that $\bar{\rho} = 1/(6\pi G t^2)$ in EdS. The terms on the right hand side of this equation now correspond to the effective stress-energy tensor from EFToLSS since smoothing these terms will give rise to products of short modes. In order to obtain an expression equivalent to Eq. 2.7, we expand the right hand side up to linear order in the long mode, keeping all orders of the short mode. Since we are keeping the short mode constant and $\delta_l = a\delta_{l,i}$, it is equivalent up to a factor of a to take derivatives with respect to the *initial* long mode. Furthermore, since also $\delta_{s,i}$ is kept constant, it is equivalent to take derivatives with respect to $\delta_i = \delta_{l,i} + \delta_{s,i}$. We obtain

$$\frac{4}{3}\frac{\dot{\delta}^2}{1+\delta} + \frac{2}{3t^2}\delta^2 = \left[\frac{8}{3}\frac{\dot{\delta}}{1+\delta}\frac{d\dot{\delta}}{d\delta_i} + \frac{4}{3}\left(\frac{\delta}{t^2} - \frac{\dot{\delta}^2}{(1+\delta)^2}\right)\frac{d\delta}{d\delta_i}\right]_{\delta_{l,i}=0}\delta_i + \mathcal{O}(\delta_i^2). \tag{6.7}$$

Next, we will calculate the functions in the above expression explicitly as functions of η. First of all, we need the derivative $d\delta_i/d\eta$. We take the derivative of $t(\eta)$ at constant time t, thus $dt/d\eta = 0$ and on the right hand side we use the product rule to obtain

$$0 = \frac{t_i}{\eta_i - \sin\eta_i}(1-\cos\eta) - \frac{t_i(1-\cos\eta_i)}{(\eta_i - \sin\eta_i)^2}\frac{d\eta_i}{d\eta}(\eta - \sin\eta), \tag{6.8}$$

thus

$$\frac{d\eta_i}{d\eta} = \frac{\eta_i - \sin\eta_i}{1-\cos\eta_i}\frac{1-\cos\eta}{\eta - \sin\eta}. \tag{6.9}$$

Furthermore, we take the derivative with respect to η of $\delta(\eta)$ (and equivalently the derivative with respect to η_i of $\delta_i = \delta(\eta_i)$) and combine this with $d\eta_i/d\eta$ to obtain

$$\frac{d\delta}{d\delta_i} = \frac{d\delta}{d\eta}\Big/\left(\frac{d\delta_i}{d\eta_i}\cdot\frac{d\eta_i}{d\eta}\right) = \frac{(1-\cos\eta_i)^5}{(1-\cos\eta)^5}\frac{(\eta-\sin\eta)^2\left[2(1-\cos\eta)^2 - 3\sin\eta(\eta-\sin\eta)\right]}{(\eta_i-\sin\eta_i)^2\left[2(1-\cos\eta_i)^2 - 3\sin\eta_i(\eta_i-\sin\eta_i)\right]}. \tag{6.10}$$

If we now expand this in terms of $\delta_i(\eta)$, we obtain

$$\frac{d\delta}{d\delta_i} = 1 + \frac{34}{21}\delta_i + \frac{341}{189}\delta_i^2 + \dots \tag{6.11}$$

which is exactly what we would expect if we would take the derivative of the perturbative expansion that we found before (see Eq. (1.22)):

$$\delta = \delta_i + \frac{17}{21}\delta_i^2 + \frac{341}{567}\delta_i^3 + \dots \tag{6.12}$$

thus we conclude that our method of taking derivatives is correct. Thus, we proceed to explicitly calculate all necessary functions using Mathematica. First, we calculate $\dot{\delta}$,

$$\begin{aligned}\dot{\delta} &= \frac{d\delta}{dt} = \frac{d\delta}{d\eta}\Big/\frac{dt}{d\eta} \\ &= \frac{9(\eta_i - \sin\eta_i)}{4t_i}\frac{(\eta-\sin\eta)\left[\cos^2\eta + 8\cos\eta - 9 - \sin^2\eta + 6\eta\sin\eta\right]}{(1-\cos\eta)^5},\end{aligned} \tag{6.13}$$

and from this it follows that

$$\begin{aligned}\frac{d\dot{\delta}}{d\delta_i} &= \frac{d\dot{\delta}}{d\eta} \Big/ \frac{d\delta_i}{d\eta} \\ &= \frac{(1-\cos\eta_i)^5}{t_i(\eta_i-\sin\eta_i)[2(1-\cos\eta_i)^2-3\sin\eta_i(\eta_i-\sin\eta_i]} \frac{(\eta-\sin\eta)}{(1-\cos\eta)^7} \cdot [15\eta^2\sin^2\eta \\ &\quad + 3\eta^2\cos^2\eta - 3\eta^2\cos\eta + 15\sin^4\eta - 30\eta\sin^3\eta + 12\sin^2\eta - 12\eta\sin\eta \\ &\quad + 2\cos^4\eta - 8\cos^3\eta + 12\cos^2\eta - 8\cos\eta + 15\sin^2\eta\cos^2\eta \\ &\quad - 18\eta\sin\eta\cos^2\eta - 27\sin^2\eta\cos\eta + 30\eta\sin\eta\cos\eta + 2].\end{aligned} \tag{6.14}$$

We now have all functions and derivatives in terms of the parameter η and the initial conditions η_i and t_i. Now, we want to take the expectation value over the initial conditions δ_i of the non-linear terms in (6.7) in order to obtain c_s^2. However, the expression is still written in terms of the parameter η and implicitly using Lagrangian coordinates. In Lagrangian coordinates, the appearance of c_s^2 in the stress-energy tensor is less clear, thus the coordinates need to be transformed to the Eulerian frame. Then, spatial derivatives will appear and it will become clear which terms represent c_s^2 and c_v^2. It should be possible to make this coordinate transformation, since we implicitly have $\delta(R)$ for all R thus in principle we have all necessary information. However, we do not know how to do this calculation explicitly so this is left as future work.

Conclusion and Outlook

The Effective Field Theory of Large Scale Structures is a theory which describes the distribution of matter in our universe as an effective fluid, with a speed of sound, viscosity and stochastic noise. These parameters can only be determined through simulations or experiments. Currently, not much is known about their precise value, but they are crucial to obtain a better understanding of large-scale structure formation. In this thesis, we have focussed on the speed of sound and viscosity. We have attempted to obtain expressions that can give us more insight into their precise value and in particular their time-dependence. We have done this by using two different approaches. First, we have calculated c_s^2 by using the perturbative approach of the EFToLSS. When doing this, we were able to check that the contributions to the power spectrum arising from the effective terms exactly cancel the divergent loop integrals from SPT.

Second, we have used a new approach, where we invoked the assumption of spherical collapse dynamics in order to obtain exact solutions to the equations of motion. Our main goal has been to develop a method that can be used to obtain analytic expressions for the effective parameters. We started with an Einstein-de Sitter universe, since for this case we already know the time-dependence of the effective parameters through self-similarity. Thus, by working in EdS, we can check whether our analytic method indeed gives rise to the correct time-dependence. We have made some progress in developing such a method. Namely, we have obtained clear spherical collapse solutions and we have derived an expression for the non-linear terms in the equation of motion that correspond to the effective stress-energy tensor from EFtoLSS. Thus, our expression implicitly contains all necessary information to obtain c_s^2, but it is still written in a parametric form in Lagrangian coordinates. To obtain an explicit expression, it needs to be rewritten to Eulerian coordinates and averaged over the initial conditions. We believe that these steps should be straightforward. The final result will be time-dependent and also explicitly dependent on the initial conditions. Our method can then be generalized to other cosmological models such as ΛCDM, in which the time-dependence becomes a bit more complicated and can be written in terms of the growth function.

One might argue that our method uses big assumptions about the matter distribution, namely the fact that it is distributed in a spherically symmetric way. It is clear that this is not the case in the real universe, but we can use this approximation in locally overdense regions and then perform a summation over such regions to obtain a description of the non-linear matter distribution. Furthermore, we can repeat our calculation for underdensities and add these to the summation to take into account the effect of voids. We can also exploit other approximations such as linear collapse and combine the different approximations in order to obtain a more realistic representation of gravitational collapse.

We believe that we can learn a lot from such a description. Namely, at present time only some numerical values of c_s^2 for one particular time are known. Exact solutions could give us insight in the evolution of the effective parameters from the primordial universe until the far future. Also, the effect of different initial conditions on the evolution of the universe could be analyzed. The results can hopefully give us great new insights in the formation of large-scale structures.

Appendix A

Alternative derivation of c_s^2

In this appendix[1], we present an alternative derivation for c_s^2. Here, we follow the method described in Appendix D from [6]. We believe that there is a mistake in their Eq. (D.10), since a first order approximation is made there, while later on second order terms appear. In this paper the effective parameters arising from EFToLSS are defined as

$$c_s^2 = \frac{1}{\bar{\rho}} \frac{\langle \delta_l p_{\text{eff}} \rangle}{\langle \delta_l \delta_l \rangle}, \quad c_v^2 = \frac{\langle \delta_l \sigma_{\text{eff}} \rangle}{\langle \delta_l \delta_l \rangle}, \quad \text{where } p_{\text{eff}} = \frac{1}{3} \langle \tau^i{}_i \rangle \text{ and } \sigma_{\text{eff}} = \frac{1}{\bar{\rho}} \frac{\partial_i \partial_j}{\partial^2} \langle [\hat{\tau}^i{}_j]^\Lambda] \rangle, \tag{A.1}$$

where $\hat{\tau}^i{}_j$ denotes the traceless part of $\tau^i{}_j$. The stress-energy tensor and its trace can be written as

$$\tau_{ij} = \rho v_i v_j - \frac{\delta_{ij}(\nabla\phi)^2 - 2\phi_{,i}\phi_{,j}}{8\pi G a^2}, \quad \tau \equiv \tau^i{}_i = \rho v^2 - \frac{(\nabla\phi)^2}{8\pi G a^2}. \tag{A.2}$$

We can now rewrite this stress-energy tensor using perturbation theory in order to calculate the effective terms. As in Ch. 5, we are only interested in the third order, because this will give rise to c_s^2 and c_v^2. Thus, we expand the stress-energy tensor up to third order in δ_1, using $\rho = \bar{\rho}(1+\delta)$, to obtain

$$\begin{aligned} \tau_{ij}^{(3)} &= \bar{\rho} \left(\delta^{(1)} v_i^{(1)} v_j^{(1)} + v_i^{(1)} v_j^{(2)} + v_i^{(2)} v_j^{(1)} \right) \\ &\quad - \frac{2\bar{\rho}}{3\mathcal{H}^2} \left(\delta_{ij} (\nabla\phi^{(1)}) \cdot (\nabla\phi^{(2)}) - \phi_{,i}^{(1)} \phi_{,j}^{(2)} - \phi_{,i}^{(2)} \phi_{,j}^{(1)} \right) \end{aligned} \tag{A.3}$$

$$\tau^{(3)} = \bar{\rho} \delta^{(1)} \mathbf{v}^{(1)} \cdot \mathbf{v}^{(1)} + 2\bar{\rho} \mathbf{v}^{(1)} \cdot \mathbf{v}^{(2)} - \frac{2\bar{\rho}}{3\mathcal{H}^2} (\nabla\phi^{(1)}) \cdot (\nabla\phi^{(2)}). \tag{A.4}$$

Using our assumption that vorticity is zero, we can write $v_i(\mathbf{x}) = \partial_i u(\mathbf{x})$. In Fourier space, this becomes

$$\mathbf{v}_{\mathbf{k}}^{(n)} = -\frac{\mathrm{i}\mathbf{k}}{k^2} \theta_{\mathbf{k}}^{(n)}, \tag{A.5}$$

and we can use this to rewrite the first two terms in A.4. For the third term, we use Poisson's equation 1.3, which takes the following form in Fourier space,

$$\phi_{\mathbf{k}}^{(n)} = -\frac{3\mathcal{H}^2}{2} \frac{1}{k^2} \delta_{\mathbf{k}}^{(n)}. \tag{A.6}$$

[1] This appendix has been made in collaboration with Nikki Bisschop, thus the same derivation also appears in his thesis.

Plugging in these expressions in Eq. A.4, we obtain

$$\begin{aligned}
\left[\tau^{(3)}\right]_\Lambda(\mathbf{p}) &= W_\Lambda(p)\int_{\mathbf{x}}\tau^{(3)}(\mathbf{x})\mathrm{e}^{-\mathrm{i}\mathbf{p}\cdot\mathbf{x}} \\
&= 2\bar{\rho}W_\Lambda(p)\int_{\mathbf{x}}\int_{\mathbf{k}}\int_{\mathbf{q}}\mathrm{e}^{-\mathrm{i}(\mathbf{p}-\mathbf{k}-\mathbf{q})\cdot\mathbf{x}}\left[\mathbf{v}^{(1)}_{\mathbf{k}}\cdot\mathbf{v}^{(2)}_{\mathbf{q}}-\frac{1}{3\mathcal{H}^2}(\mathrm{i}\mathbf{k})\cdot(\mathrm{i}\mathbf{q})\phi^{(1)}_{\mathbf{k}}\phi^{(2)}_{\mathbf{q}}\right] \\
&\quad+\bar{\rho}W_\Lambda(p)\int_{\mathbf{x}}\int_{\mathbf{q}}\int_{\mathbf{q}_1}\int_{\mathbf{q}_2}\mathrm{e}^{-\mathrm{i}(\mathbf{p}-\mathbf{q}-\mathbf{q}_1-\mathbf{q}_2)\cdot\mathbf{x}}\delta^{(1)}_{\mathbf{q}}\mathbf{v}^{(1)}_{\mathbf{q}_1}\cdot\mathbf{v}^{(1)}_{\mathbf{q}_2} \\
&= 2\bar{\rho}W_\Lambda(p)\int_{\mathbf{q}}\alpha(\mathbf{q},\mathbf{p})\left[-\theta^{(1)}_{\mathbf{p}-\mathbf{q}}\theta^{(2)}_{\mathbf{q}}+\frac{3\mathcal{H}^2}{4}\delta^{(1)}_{\mathbf{p}-\mathbf{q}}\delta^{(2)}_{\mathbf{q}}\right] \\
&\quad-\bar{\rho}W_\Lambda(p)\int_{\mathbf{q}}\int_{\mathbf{q}_1}\int_{\mathbf{q}_2}\frac{\mathbf{q}_1\cdot\mathbf{q}_2}{q_1^2q_2^2}\delta^{(1)}_{\mathbf{p}-\mathbf{q}}\theta^{(1)}_{\mathbf{q}_1}\theta^{(1)}_{\mathbf{q}_2}\delta_D(\mathbf{q}-\mathbf{q}_1-\mathbf{q}_2) \\
&= -\frac{1}{2}\bar{\rho}\mathcal{H}^2W_\Lambda(p)\int_{\mathbf{q}}\int_{\mathbf{q}_1}\int_{\mathbf{q}_2}\alpha(\mathbf{q},\mathbf{p})H_2(\mathbf{q}_1,\mathbf{q}_2)\delta^{(1)}_{\mathbf{p}-\mathbf{q}}\delta^{(1)}_{\mathbf{q}_1}\delta^{(1)}_{\mathbf{q}_2}\delta_D(\mathbf{q}-\mathbf{q}_1-\mathbf{q}_2) \\
&\quad-\bar{\rho}\mathcal{H}^2W_\Lambda(p)\int_{\mathbf{q}}\int_{\mathbf{q}_1}\int_{\mathbf{q}_2}\frac{\mathbf{q}_1\cdot\mathbf{q}_2}{q_1^2q_2^2}\delta^{(1)}_{\mathbf{p}-\mathbf{q}}\delta^{(1)}_{\mathbf{q}_1}\delta^{(1)}_{\mathbf{q}_2}\delta_D(\mathbf{q}-\mathbf{q}_1-\mathbf{q}_2)
\end{aligned}$$

where α is defined slightly different compared to Eq. 1.13, namely

$$\alpha(\mathbf{q},\mathbf{p})=\frac{(\mathbf{p}-\mathbf{q})\cdot\mathbf{q}}{(\mathbf{p}-\mathbf{q})^2q^2}, \tag{A.7}$$

and

$$H_2(\mathbf{q}_1,\mathbf{q}_2)=4G_2(\mathbf{q}_1,\mathbf{q}_2)-3F_2(\mathbf{q}_1,\mathbf{q}_2)=-\frac{3}{7}+\frac{1}{2}\mu\left(\frac{q_1}{q_2}+\frac{q_2}{q_1}\right)+\frac{10}{7}. \tag{A.8}$$

To obtain c_s^2, we first need to compute

$$\begin{aligned}
\langle\delta^{(1)}_{\mathbf{k}}[\tau]^\Lambda_{\mathbf{p}}\rangle &= -\frac{1}{2}\bar{\rho}\mathcal{H}^2W_\Lambda(p)\int_{\mathbf{q}}\int_{\mathbf{q}_1}\int_{\mathbf{q}_2}\alpha(\mathbf{q},\mathbf{p})H_2(\mathbf{q}_1,\mathbf{q}_2)\delta_D(\mathbf{q}-\mathbf{q}_1-\mathbf{q}_2)\langle\delta^{(1)}_{\mathbf{k}}\delta^{(1)}_{\mathbf{p}-\mathbf{q}}\delta^{(1)}_{\mathbf{q}_1}\delta^{(1)}_{\mathbf{q}_2}\rangle. \\
&\quad-\bar{\rho}\mathcal{H}^2W_\Lambda(p)\int_{\mathbf{q}}\int_{\mathbf{q}_1}\int_{\mathbf{q}_2}\frac{\mathbf{q}_1\cdot\mathbf{q}_2}{q_1^2q_2^2}\delta_D(\mathbf{q}-\mathbf{q}_1-\mathbf{q}_2)\langle\delta^{(1)}_{\mathbf{k}}\delta^{(1)}_{\mathbf{p}-\mathbf{q}}\delta^{(1)}_{\mathbf{q}_1}\delta^{(1)}_{\mathbf{q}_2}\rangle.
\end{aligned} \tag{A.9}$$

Assuming Gaussian initial conditions, we use Wick's theorem to rewrite the 4-point function,

$$\begin{aligned}
\langle\delta^{(1)}_{\mathbf{k}}\delta^{(1)}_{\mathbf{p}-\mathbf{q}}\delta^{(1)}_{\mathbf{q}_1}\delta^{(1)}_{\mathbf{q}_2}\rangle &= \langle\delta^{(1)}_{\mathbf{k}}\delta^{(1)}_{\mathbf{p}-\mathbf{q}}\rangle\langle\delta^{(1)}_{\mathbf{q}_1}\delta^{(1)}_{\mathbf{q}_2}\rangle+\langle\delta^{(1)}_{\mathbf{k}}\delta^{(1)}_{\mathbf{q}_1}\rangle\langle\delta^{(1)}_{\mathbf{p}-\mathbf{q}}\delta^{(1)}_{\mathbf{q}_2}\rangle+\langle\delta^{(1)}_{\mathbf{k}}\delta^{(1)}_{\mathbf{q}_2}\rangle\langle\delta^{(1)}_{\mathbf{p}-\mathbf{q}}\delta^{(1)}_{\mathbf{q}_1}\rangle \\
&= \delta_D(\mathbf{k}+\mathbf{p}-\mathbf{q})\delta_D(\mathbf{q}_1+\mathbf{q}_2)P_\delta(k)P_\delta(q_1) && \text{(A.10)} \\
&\quad+\delta_D(\mathbf{k}+\mathbf{q}_1)\delta_D(\mathbf{p}-\mathbf{q}+\mathbf{q}_2)P_\delta(k)P_\delta(|\mathbf{p}-\mathbf{q}|) && \text{(A.11)} \\
&\quad+\delta_D(\mathbf{k}+\mathbf{q}_2)\delta_D(\mathbf{p}-\mathbf{q}+\mathbf{q}_1)P_\delta(k)P_\delta(|\mathbf{p}-\mathbf{q}|). && \text{(A.12)}
\end{aligned}$$

We now integrate the first term of Eq. A.9 over $\mathbf{q}_1$ and $\mathbf{q}_2$. Because $H_2(\mathbf{q}_1,\mathbf{q}_2)$ is symmetric under exchange of $\mathbf{q}_1$ and $\mathbf{q}_2$, the last two terms give the same contribution,

$$\begin{aligned}
&\int_{\mathbf{q}_1}\int_{\mathbf{q}_2}H_2(\mathbf{q}_1,\mathbf{q}_2)\delta_D(\mathbf{q}-\mathbf{q}_1-\mathbf{q}_2)\langle\delta^{(1)}_{\mathbf{k}}\delta^{(1)}_{\mathbf{p}-\mathbf{q}}\delta^{(1)}_{\mathbf{q}_1}\delta^{(1)}_{\mathbf{q}_2}\rangle \\
&\qquad= 2\delta_D(\mathbf{p}+\mathbf{k})P_\delta(k)H_2(-\mathbf{k},\mathbf{k}+\mathbf{q})P_\delta(|\mathbf{p}-\mathbf{q}|) \\
&\qquad\quad+\delta_D(\mathbf{q})\delta(\mathbf{p}+\mathbf{k})P_\delta(k)\int_{\mathbf{q}'}H_2(\mathbf{q}',-\mathbf{q}')P_\delta(\mathbf{q}') \\
&\qquad= 2\langle\delta^{(1)}_{\mathbf{k}}\delta^{(1)}_{\mathbf{p}}\rangle H_2(-\mathbf{k},\mathbf{k}+\mathbf{q})P_\delta(|\mathbf{p}-\mathbf{q}|) \\
&\qquad\quad+\langle\delta^{(1)}_{\mathbf{k}}\delta^{(2)}_{\mathbf{p}}\rangle\delta_D(q)\int_{\mathbf{q}'}H_2(\mathbf{q}',-\mathbf{q}')P_\delta(\mathbf{q}'),
\end{aligned} \tag{A.13}$$

and the second term of Eq. A.9 becomes

$$\begin{aligned}\int_{\mathbf{q}_1}\int_{\mathbf{q}_2}\frac{\mathbf{q}_1\cdot\mathbf{q}_2}{q_1^2q_2^2}\delta_D(\mathbf{q}-\mathbf{q}_1-\mathbf{q}_2)\langle\delta^{(1)}_{\mathbf{k}}\delta^{(1)}_{\mathbf{p}-\mathbf{q}}\delta^{(1)}_{\mathbf{q}_1}\delta^{(1)}_{\mathbf{q}_2}\rangle&\\ =-2\alpha(\mathbf{p},\mathbf{q})\delta_D(\mathbf{p}+\mathbf{k})P_\delta(k)P_\delta(|\mathbf{p}-\mathbf{q}|)&\\ -\delta_D(q)\delta_D(\mathbf{p}+\mathbf{k})P_\delta(k)\int_{\mathbf{q}'}\frac{1}{q'^2}P_\delta(q')&\quad(A.14)\\ =-2\langle\delta^{(1)}_{\mathbf{k}}\delta^{(1)}_{\mathbf{p}}\rangle\alpha(\mathbf{p},\mathbf{q})P_\delta(|\mathbf{p}-\mathbf{q}|)&\\ -\langle\delta^{(1)}_{\mathbf{k}}\delta^{(1)}_{\mathbf{p}}\rangle\delta_D(q)\int_{\mathbf{q}'}\frac{1}{q'^2}P_\delta(q').&\quad(A.15)\end{aligned}$$

Plugging it all in, we obtain

$$\begin{aligned}\langle\delta^{(1)}_{\mathbf{k}}[\tau]^\Lambda_{\mathbf{p}}\rangle=-\bar\rho\mathcal{H}^2W_\Lambda(k)\langle\delta^{(1)}_{\mathbf{k}}\delta^{(1)}_{\mathbf{p}}\rangle\int_{\mathbf{q}}\left\{\alpha(\mathbf{q},-\mathbf{k})H_2(-\mathbf{k},\mathbf{k}+\mathbf{q})-2\alpha(-\mathbf{k},\mathbf{q})\right\}P_\delta(|\mathbf{k}+\mathbf{q}|)&\\ -\frac{1}{2}\bar\rho\mathcal{H}^2W_\Lambda(k)\langle\delta^{(1)}_{\mathbf{k}}\delta^{(1)}_{\mathbf{p}}\rangle\int_{\mathbf{q}}\left[H_2(\mathbf{q},-\mathbf{q})-\frac{2}{q^2}\right]P_\delta(q)&\quad(A.16)\\ =-\bar\rho\mathcal{H}^2W_\Lambda(k)\langle\delta^{(1)}_{\mathbf{k}}\delta^{(1)}_{\mathbf{p}}\rangle\int_{\mathbf{q}}\left\{\alpha(\mathbf{q}-\mathbf{k},-\mathbf{k})H_2(-\mathbf{k},\mathbf{q})-2\alpha(-\mathbf{k},\mathbf{q}-\mathbf{k})\right\}P_\delta(q)&\\ +\bar\rho\mathcal{H}^2W_\Lambda(k)\langle\delta^{(1)}_{\mathbf{k}}\delta^{(1)}_{\mathbf{p}}\rangle\int_{\mathbf{q}}\frac{1}{q^2}P_\delta(q)&\quad(A.17)\\ =-\bar\rho\mathcal{H}^2W_\Lambda(k)\langle\delta^{(1)}_{\mathbf{k}}\delta^{(1)}_{\mathbf{p}}\rangle\int_{\mathbf{q}}\Bigg\{\alpha(\mathbf{q}-\mathbf{k},-\mathbf{k})H_2(-\mathbf{k},\mathbf{q})&\quad(A.18)\\ -2\alpha(-\mathbf{k},\mathbf{q}-\mathbf{k})-\frac{1}{q^2}\Bigg\}P_\delta(q)&\quad(A.19)\end{aligned}$$

Since $\delta^{(1)}_{\mathbf{k}}$ represents a long mode, we take the limit $k\ll q$, thus we expand around $k=0$,

$$\begin{aligned}\alpha(\mathbf{q}-\mathbf{k},-\mathbf{k})H_2(-\mathbf{k},\mathbf{q})-2\alpha(-\mathbf{k},\mathbf{q}-\mathbf{k})-\frac{1}{q^2}&\\ =\left[-\frac{1}{q^2}-\mu\frac{k}{q^3}+\mathcal{O}(k^2)\right]\times\left[-\frac{3}{7}-\frac{1}{2}\mu\frac{q}{k}+\frac{10}{7}\mu^2+\mathcal{O}(k)\right]-2\mu\frac{1}{kq}-\frac{1}{q^2}&\\ =-\frac{1}{q^2}\left(\frac{4}{7}+\frac{13}{14}\mu^2+\mathcal{O}(k)\right)+\text{terms linear in }\mu&\quad(A.20)\end{aligned}$$

where

$$\mu=\frac{\mathbf{k}\cdot\mathbf{q}}{kq}$$

and hence c_s^2 becomes

$$\begin{aligned}c_s^2=\frac{1}{3\bar\rho}\frac{\langle\delta^{(1)}_{\mathbf{k}}[\tau]^\Lambda_{\mathbf{p}}\rangle}{\langle\delta^{(1)}_{\mathbf{k}}\delta^{(1)}_{\mathbf{p}}\rangle}=\frac{1}{3}\mathcal{H}^2\int_{\mathbf{q}}\frac{1}{q^2}\left(\frac{4}{7}+\frac{13}{14}\mu^2\right)P_\delta(q)&\\ =\frac{1}{3}\frac{1}{(2\pi)^2}\mathcal{H}^2\int dq\;P_\delta(q)\int_{-1}^{1}d\mu\;\left(\frac{4}{7}+\frac{13}{14}\mu^2\right)&\quad(A.21)\\ =\frac{37}{126}\frac{1}{2\pi^2}\mathcal{H}^2\int dq\;P_\delta(q)&\quad(A.22)\end{aligned}$$

At first order, $\theta_{\mathbf{k}}^{(1)} = -\mathcal{H}\delta_{\mathbf{k}}^{(1)}$ but for second order this does not hold, $\theta_{\mathbf{k}}^{(2)} \neq -\mathcal{H}\delta_{\mathbf{k}}^{(2)}$. In [6], this is implicitly used, thus this is where our calculation is different. In their calculation, in the previous expressions F_2 appears instead of H_2.

The steps in the calculation of c_v^2 are the same, but now starting from A.3,

$$\begin{aligned}\left[\hat{\tau}_{ij}^{(3)}\right]_\Lambda(\mathbf{p}) = W_\Lambda(p)\int_{\mathbf{k}}\int_{\mathbf{q}}\Bigg\{&\bar{\rho}\left(\left(v_{\mathbf{k}}^{(1)}\right)_i\left(v_{\mathbf{q}}^{(2)}\right)_j + \left(v_{\mathbf{k}}^{(2)}\right)_i\left(v_{\mathbf{q}}^{(1)}\right)_j - \frac{2}{3}\delta_{ij}\mathbf{v}_{\mathbf{k}}^{(1)}\cdot\mathbf{v}_{\mathbf{q}}^{(2)}\right)\\ &+\frac{2\bar{\rho}}{3\mathcal{H}^2}\left(\frac{2}{3}\delta_{ij}(\mathbf{k}\cdot\mathbf{q}) - k_iq_j - k_jq_i\right)\phi_{\mathbf{k}}^{(1)}\phi_{\mathbf{q}}^{(2)}\Bigg\}\delta_D(\mathbf{p}-\mathbf{q}-\mathbf{k})\\ &+W_\Lambda(p)\bar{\rho}\int_{\mathbf{q}}\int_{\mathbf{q}_1}\int_{\mathbf{q}_2}\left\{\delta_{\mathbf{q}}^{(1)}\left(v_{\mathbf{q}_1}^{(1)}\right)_i\left(v_{\mathbf{q}_2}^{(1)}\right)_j - \frac{1}{3}\delta_{ij}\delta_{\mathbf{q}}^{(1)}\mathbf{v}_{\mathbf{q}_1}^{(1)}\cdot\mathbf{v}_{\mathbf{q}_2}^{(1)}\right\}\delta_D(\mathbf{p}-\mathbf{q}-\mathbf{q}_1-\mathbf{q}_2)\end{aligned} \tag{A.23}$$

$$\begin{aligned}&= -2\bar{\rho}W_\Lambda(p)\int_{\mathbf{q}}\left\{\frac{(p_i-q_i)q_j - \frac{1}{3}\delta_{ij}(\mathbf{p}-\mathbf{q})\cdot\mathbf{q}}{(\mathbf{p}-\mathbf{q})^2q^2}\left(\theta_{\mathbf{p}-\mathbf{q}}^{(1)}\theta_{\mathbf{q}}^{(2)} + \frac{3\mathcal{H}^2}{2}\delta_{\mathbf{p}-\mathbf{q}}^{(1)}\delta_{\mathbf{q}}^{(2)}\right)\right\}\\ &\quad + W_\Lambda(p)\bar{\rho}\int_{\mathbf{q}}\int_{\mathbf{q}_1}\int_{\mathbf{q}_2}\frac{q_1^iq_2^j - \frac{1}{3}\delta_{ij}\mathbf{q}_1\cdot\mathbf{q}_2}{q_1^2q_2^2}\delta_{\mathbf{q}}^{(1)}\theta_{\mathbf{q}_1}^{(1)}\theta_{\mathbf{q}_2}^{(1)}\delta_D(\mathbf{p}-\mathbf{q}-\mathbf{q}_1-\mathbf{q}_2)\end{aligned} \tag{A.24}$$

$$\begin{aligned}&= -5\bar{\rho}\mathcal{H}^2W_\Lambda(p)\int_{\mathbf{q}}\int_{\mathbf{q}_1}\int_{\mathbf{q}_2}\beta_{ij}(\mathbf{q},\mathbf{p})\tilde{H}_2(\mathbf{q}_1,\mathbf{q}_2)\delta_{\mathbf{p}-\mathbf{q}}^{(1)}\delta_{\mathbf{q}_1}^{(1)}\delta_{\mathbf{q}_2}^{(1)}\\ &\quad + \bar{\rho}\mathcal{H}^2W_\Lambda(p)\int_{\mathbf{q}}\int_{\mathbf{q}_1}\int_{\mathbf{q}_2}\frac{q_1^iq_2^j - \frac{1}{3}\delta_{ij}\mathbf{q}_1\cdot\mathbf{q}_2}{q_1^2q_2^2}\delta_{\mathbf{q}}^{(1)}\delta_{\mathbf{q}_1}^{(1)}\delta_{\mathbf{q}_2}^{(1)}\delta_D(\mathbf{p}-\mathbf{q}-\mathbf{q}_1-\mathbf{q}_2),\end{aligned} \tag{A.25}$$

where,

$$\beta_{ij}(\mathbf{q},\mathbf{p}) = \frac{(p_i-q_i)q_j - \frac{1}{3}\delta_{ij}(\mathbf{p}-\mathbf{q})\cdot\mathbf{q}}{(\mathbf{p}-\mathbf{q})^2q^2}, \tag{A.26}$$

$$\tilde{H}_2(\mathbf{q}_1,\mathbf{q}_2) = \frac{2}{5}G_2(\mathbf{q}_1,\mathbf{q}_2) + \frac{3}{5}F_2(\mathbf{q}_1,\mathbf{q}_2) = \frac{3}{5} + \frac{1}{2}\mu\left(\frac{q_1}{q_2}+\frac{q_2}{q_1}\right) + \frac{2}{5}\mu^2. \tag{A.27}$$

Using the results from the previous calculation, we obtain

$$\begin{aligned}\langle\delta_\ell\sigma_{\text{eff}}\rangle &= \frac{1}{\bar{\rho}}\left\langle\delta_{\mathbf{k}}^\ell\frac{p_ip_j}{p^2}\left[\hat{\tau}_{ij}^{(3)}\right]_{\mathbf{p}}^\Lambda\right\rangle\\ &= -10\mathcal{H}^2W_\Lambda(k)\langle\delta_{\mathbf{k}}^{(1)}\delta_{\mathbf{p}}^{(1)}\rangle\int_{\mathbf{q}}\beta(\mathbf{q},-\mathbf{k})\tilde{H}_2(-\mathbf{k},\mathbf{k}+\mathbf{q})P_\delta(|\mathbf{p}-\mathbf{q}|),\\ &\quad + \mathcal{H}^2W_\Lambda(p)\int_{\mathbf{q}}\int_{\mathbf{q}_1}\int_{\mathbf{q}2}\frac{(\mathbf{p}\cdot\mathbf{q}_1)(\mathbf{p}\cdot\mathbf{q}_2) - \frac{1}{3}p^2\mathbf{q}_1\cdot\mathbf{q}_2}{p^2q_1^2q_2^2}\langle\delta_{\mathbf{k}}^{(1)}\delta_{\mathbf{p}-\mathbf{q}}^{(1)}\delta_{\mathbf{q}_1}^{(1)}\delta_{\mathbf{q}_2}^{(1)}\rangle\delta_D(\mathbf{q}-\mathbf{q}_1-\mathbf{q}_2)\end{aligned} \tag{A.28}$$

$$\begin{aligned}&= -10\mathcal{H}^2W_\Lambda(k)\langle\delta_{\mathbf{k}}^{(1)}\delta_{\mathbf{p}}^{(1)}\rangle\int_{\mathbf{q}}\beta(\mathbf{q}-\mathbf{k},-\mathbf{k})\tilde{H}_2(-\mathbf{k},\mathbf{q})P_\delta(q),\\ &\quad - \mathcal{H}^2W_\Lambda(p)\langle\delta_{\mathbf{k}}^{(1)}\delta_{\mathbf{p}}^{(1)}\rangle\int_{\mathbf{q}}\frac{1}{q^2}\underbrace{\left[\frac{1}{3} - \frac{q}{p}\mu - \mu^2\right]}_{=0\text{ after angular integration}}P_\delta(q)\end{aligned} \tag{A.29}$$

where β is also defined slightly different, namely

$$\beta(\mathbf{q},\mathbf{p}) \equiv \frac{p_ip_j}{p^2}\beta_{ij}(\mathbf{q},\mathbf{p}) = \frac{\mathbf{p}\cdot(\mathbf{p}-\mathbf{q})\mathbf{p}\cdot\mathbf{q} - \frac{1}{3}p^2(\mathbf{p}-\mathbf{q})\cdot\mathbf{q}}{p^2q^2(\mathbf{p}-\mathbf{q})^2}. \tag{A.30}$$

Taking the limit $k \ll q$, we obtain

$$\begin{aligned}\beta(\mathbf{q}-\mathbf{k},-\mathbf{k})\tilde{H}_2(-\mathbf{k},\mathbf{q}) \\ &= -\frac{1}{q^2}\left[-\frac{1}{3}-\frac{4}{3}\mu\frac{k}{q}+\mu^2+2\mu^3\frac{k}{q}\right]\times\left[\frac{3}{5}-\frac{1}{2}\mu\frac{q}{k}+\frac{2}{5}\mu^2\right] \\ &= -\frac{1}{q^2}\left[-\frac{1}{5}+\frac{17}{15}\mu^2-\frac{3}{5}\mu^4+\mathcal{O}(k)\right]+\text{ terms of odd order in }\mu \end{aligned} \tag{A.31}$$

and thus,

$$\begin{aligned} c_v^2 &\equiv \frac{\langle\delta_l\sigma_{\rm eff}\rangle}{\langle\delta_l\delta_l\rangle} = 10\mathcal{H}^2\frac{1}{(2\pi)^2}\int_{\mathbf{q}}\frac{1}{q^2}\left[-\frac{1}{5}+\frac{17}{15}\mu^2-\frac{3}{5}\mu^4\right]P_\delta(q) \\ &= \frac{26}{45}\frac{1}{2\pi^2}\mathcal{H}^2\int dq\ P_\delta(q), \end{aligned} \tag{A.32}$$

and we finally obtain

$$c_{\rm comb}^2 = c_s^2+c_v^2 = \frac{61}{70}\frac{1}{2\pi^2}\mathcal{H}^2\int dq\ P_\delta(q), \tag{A.33}$$

which agrees with the value that was found in Ch. 5.

A.1 Cancellation of the P_{13} UV-divergence

Now we want to check whether the divergent part of P_{13} is indeed cancelled by $P_{c_s^2}$. To compute $P_{c_s^2}$ we again start with Eq. 5.11 and use the Green's function Eq. 5.8,

$$\begin{aligned}\delta_{c_s^2} &= \int d\tilde{a}\ G(a,\tilde{a})k^2(c_s^2+c_v^2\tilde{a}\partial_{\tilde{a}})\delta_1 \\ &\overset{\rm EdS}{=} -\frac{a}{9\mathcal{H}_0^2}k^2c_{\rm comb}^2\delta_1, \end{aligned} \tag{A.34}$$

from which we obtain

$$\begin{aligned}\langle\delta_{\mathbf{k}}^{(1)}\delta_{c_s^2}(\mathbf{p})\rangle &= -\frac{a}{9\mathcal{H}_0^2}p^2c_{\rm comb}^2\langle\delta_{\mathbf{k}}^{(1)}\delta_{\mathbf{p}}^{(1)}\rangle \\ &= -\frac{61a}{630\pi^2}\frac{\mathcal{H}^2}{\mathcal{H}_0^2}p^2\delta_D(\mathbf{k}+\mathbf{p})P_\delta(k)\int dq\ P_\delta(q), \end{aligned} \tag{A.35}$$

and thus

$$P_{c_s^2}(k) = -\frac{61}{630\pi^2}k^2P_\delta(k)\int dq\ P_\delta(q) \tag{A.36}$$

We now assume that the primordial power spectrum follows a power law with spectral index n, i.e., $P_\delta(k) = Ak^n$. For $n \geq 0$, we obtain

$$P_{c_s^2}(k) = -\frac{1}{(2\pi)^3}\frac{244}{315}\pi A^2k^{2+n}\int_0^{k_c}dq\ q^n = -\frac{1}{(2\pi)^3}\frac{244}{315(n+1)}\pi A^2k^{2+n}k_c^{n+1}\,. \tag{A.37}$$

This is the right number to cancel the divergent part of P_{13} (see e.g. Eq. (4.36) and (4.14) of [19]),

$$P_{13}^{\rm div}(k) = \frac{61}{630\pi^2}\pi A^2k^{2+n}\int_0^{k_c}dq\ q^n \tag{A.38}$$

$$= \frac{1}{(2\pi)^3}\frac{244}{315}\pi A^2k^{2+n}\int_0^{k_c}dq\ q^n = \frac{1}{(2\pi)^3}\frac{244}{315(n+1)}\pi A^2k^{2+n}k_c^{n+1}\,. \tag{A.39}$$

This also agrees with Table 5 of [3].

Bibliography

[1] S. Dodelson, *Modern cosmology*. Academic press, 2003.

[2] W. J. Percival, "Large scale structure observations," *Lectures given to the Fermi School on "New Horizons for Observational Cosmology"*, 2013.

[3] F. Bernardeau, S. Colombi, E. Gaztanaga, and R. Scoccimarro, "Large-scale structure of the universe and cosmological perturbation theory," *Physics Reports*, vol. 367, no. 1, pp. 1–248, 2002.

[4] `http://pages.uoregon.edu/jimbrau/astr123/Notes/Chapter27.html`. Accessed: 2015-06-11.

[5] P. Murdin, "Encyclopedia of astronomy and astrophysics," *Encyclopedia of Astronomy and Astrophysics*, vol. 1, 2002.

[6] D. Baumann, A. Nicolis, L. Senatore, and M. Zaldarriaga, "Cosmological non-linearities as an effective fluid," *Journal of Cosmology and Astroparticle Physics*, vol. 2012, no. 07, p. 051, 2012.

[7] J. J. M. Carrasco, M. P. Hertzberg, and L. Senatore, "The effective field theory of cosmological large scale structures," *Journal of High Energy Physics*, vol. 2012, no. 9, pp. 1–40, 2012.

[8] E. Pajer and M. Zaldarriaga, "On the renormalization of the effective field theory of large scale structures," *Journal of Cosmology and Astroparticle Physics*, vol. 2013, no. 08, p. 037, 2013.

[9] A. Kehagias and A. Riotto, "Symmetries and consistency relations in the large scale structure of the universe," *Nuclear Physics B*, vol. 873, no. 3, pp. 514–529, 2013.

[10] S. Engineer, N. Kanekar, and T. Padmanabhan, "Non-linear density evolution from an improved spherical collapse model," *Monthly Notices of the Royal Astronomical Society*, vol. 314, no. 2, pp. 279–289, 2000.

[11] "Lecture notes on the spherical collapse model." `http://www.uio.no/studier/emner/matnat/astro/AST4320/h12/undervisningsmateriale/spherecollapse.pdf`. Accessed: 2015-06-08.

[12] `http://wigglez.swin.edu.au`. Accessed: 2015-05-28.

[13] `http://www.sdss.org`. Accessed: 2015-05-28.

[14] `http://www.2dfgrs.net`. Accessed: 2015-05-28.

[15] `http://kids.strw.leidenuniv.nl`. Accessed: 2015-05-28.

[16] `http://www.euclid-ec.org`. Accessed: 2015-05-28.

[17] `http://desi.lbl.gov`. Accessed: 2015-05-28.

[18] L. Mercolli and E. Pajer, "On the velocity in the effective field theory of large scale structures," *Journal of Cosmology and Astroparticle Physics*, vol. 2014, no. 03, p. 006, 2014.

[19] V. Assassi, D. Baumann, E. Pajer, Y. Welling, and D. van der Woude, "Effective theory of large-scale structure with primordial non-gaussianity," *arXiv preprint arXiv:1505.06668*, 2015.